ANNUAL REVIEWS

Annual Review of Materials Research

Dynamic Nuclear Polarization Solid-State NMR Spectroscopy for Materials Research

Ilia B. Moroz and Michal Leskes

Department of Molecular Chemistry and Materials Science, Weizmann Institute of Science, Rehovot, Israel; email: michal.leskes@weizmann.ac.il

Annu. Rev. Mater. Res. 2022. 52:25–55

First published as a Review in Advance on March 8, 2022

The *Annual Review of Materials Research* is online at matsci.annualreviews.org

https://doi.org/10.1146/annurev-matsci-081720-085634

Keywords

DNP, dynamic nuclear polarization, solid-state NMR, sensitivity enhancement, polarizing agents, surface sensitivity, DNP mechanisms

Abstract

Solid-state nuclear magnetic resonance (NMR) spectroscopy has increasingly been used for materials characterization as it enables selective detection of elements of interest, as well as their local structure and dynamic properties. Nevertheless, utilization of NMR is limited by its inherent low sensitivity. The development of dynamic nuclear polarization (DNP) approaches, which provide enormous sensitivity gain in NMR through the transfer of polarization from electron spins, has transformed the application of solid-state NMR in materials science. In this review, we outline the opportunities for materials characterization that DNP has opened up. We describe the main DNP mechanisms available, their implementation, and the kinds of insight they can provide across different materials classes, from surfaces and interfaces to defects in the bulk of solids. Finally, we discuss the current limitations of the approach and provide an outlook on future developments for DNP-enhanced NMR spectroscopy in materials science.

1. INTRODUCTION

Solid-state nuclear magnetic resonance (NMR) spectroscopy is a powerful characterization tool for materials science. First, it is a local technique that provides atomic-scale information on the chemical environment of the observed nuclei. Second, in contrast to X-ray diffraction methods, solid-state NMR can be applied not only to crystalline but also to amorphous and disordered materials, as well as to surfaces and interfaces. Third, it is an almost universal method as most of the elements in the periodic table have NMR active isotopes and hence can, in principle, be detected by NMR spectroscopy. Finally, NMR spectroscopy is an active research field, with new methods being developed to address specific challenges associated with the invention of new materials with new functionalities.

The main drawback of NMR spectroscopy that limits the extent of its applications is an inherently low sensitivity. This is caused by the minute population difference between nuclear spin states, which results in low signal intensity. Despite the development of experiments that can improve the signal-to-noise ratio (SNR) in NMR and reduce the experimental time (e.g., cross-polarization), it is still very challenging to obtain information about species present in low quantities (defects, active sites in heterogeneous catalysts, surface species, etc.) and/or isotopes with low gyromagnetic ratio γ (^{14}N, ^{15}N, ^{17}O, ^{35}Cl, ^{43}Ca, ^{89}Y, etc.), low natural abundance (^{13}C, ^{15}N, ^{17}O, ^{29}Si, etc.) or broad line shapes due to anisotropic chemical shielding (^{77}Se, ^{111}Cd, ^{113}Cd, ^{119}Sn, ^{195}Pt, etc.) and/or quadrupolar (^{17}O, ^{27}Al, ^{35}Cl, ^{51}V, ^{79}Br, etc.) interactions.

In the past decade, the sensitivity limitation has been practically eliminated and the field of magnetic resonance has been revolutionized by the development of hyperpolarization techniques such as dynamic nuclear polarization (DNP). In DNP the high spin polarization of unpaired electrons is transferred to the surrounding nuclear spins via microwave irradiation. This boosts NMR sensitivity by several orders of magnitude (10–10^4), opening new opportunities and expanding the range of applications for NMR spectroscopy. DNP was experimentally demonstrated in the 1950s (1); however it was initially limited to low magnetic fields. A few decades later, Griffin and colleagues (2) introduced the instrumentation that made DNP applicable at high fields combined with magic angle spinning (MAS). This includes (*a*) high-power microwave sources operating at frequencies higher than 140 GHz and (*b*) cryogenic MAS probes that can operate at 100 K and below. The commercialization of MAS DNP systems facilitated the rapid development of this method in the last decade, which led to the flourishing of MAS DNP in the fields of structural biology and materials science. The contribution of MAS DNP to materials research through solid-state NMR cannot be overstated: The sensitivity gains from DNP enable detecting materials and species that were otherwise invisible to NMR, from surface sites to bulk defects. As such, it has already been applied to a wide range of materials used for important applications, including catalysis, energy storage and conversion, pharmaceuticals, and cement, and further expansion in methodology and application can be expected in the coming years.

In this review, we focus on the application of DNP to materials. We do not review the various NMR methodologies and their capabilities in materials characterization; for that we refer the reader to a recent review by Chien et al. (3). Our aim here is to familiarize the reader with the different approaches for increasing NMR sensitivity through DNP and review the kind of information that can be gained depending on the type of the material of interest.

We first describe the basic principles of DNP and summarize the main mechanisms of the polarization transfer process. We then provide an overview of the progress brought by the application of high-field MAS DNP to materials research, divided into materials classes: surfaces and interfaces, porous materials, bulk inorganic materials, polymers, and pharmaceuticals. Finally, we discuss the current limitations of DNP and demonstrate recent findings that should help to overcome these limitations and lead to new opportunities in the future.

2. HIGH-FIELD MAGIC ANGLE SPINNING DNP

As mentioned above, the main limitation of solid-state NMR spectroscopy arises from its intrinsically low sensitivity. The intensity of the NMR signal is proportional to the population difference between the nuclear spin energy levels, which is given by the Boltzmann distribution,

$$\frac{N_\alpha}{N_\beta} = \exp\left(\frac{\hbar\gamma_I B_0}{k_B T}\right), \quad 1.$$

where $\hbar$ is the Planck constant, γ_I is the gyromagnetic ratio specific for the nuclear isotope, B_0 is the external magnetic field, k_B is the Boltzmann constant, and T is the temperature. When characterizing inorganic materials, nuclei of interest often have low gyromagnetic ratios. Moreover, their signals can be broadened due to anisotropic interactions leading to even worse SNR. The SNR is improved in NMR by repeating the experiment multiple times and accumulating the signal. However, SNR grows as the square root of the number of repetitions, which may result in extremely long experimental times that are often not feasible. It is even more of an issue for inorganic materials where nuclei often require a long time to return to their thermal equilibrium (the process of nuclear relaxation), thus requiring longer delays between repetitions to record an NMR signal. A brute force approach to increasing NMR sensitivity is to use high magnetic fields and low temperatures (see Equation 1). Another way to increase the SNR is to measure NMR in non-Boltzmann conditions, meaning that an excess of nuclear spin polarization is created, so-called hyperpolarization. One of the techniques that can provide nuclear hyperpolarization is DNP. DNP benefits from the very high electron polarization that surpasses nuclear polarization by 2–3 orders of magnitude. When an unpaired electron and a nucleus of interest are close enough to have spin–spin interactions, the electron polarization can be transferred to the nucleus using microwave irradiation, thus enhancing the NMR signal. The theoretical enhancement (ε) that can be achieved by DNP is equal to γ_e/γ_I, where γ_e is the electron gyromagnetic ratio. For ^{1}H nuclei, $\varepsilon \approx 660$, while for other nuclei the theoretical enhancement is even higher. This translates into tremendous experimental time savings.

The following components are needed in order to apply DNP for materials characterization: (*a*) a source of unpaired electrons, the so-called polarizing agent (PA), that can be added from outside (exogenous approach) or introduced into the material during or postsynthesis (endogenous approach); (*b*) a source of microwave irradiation operating at high frequency (typically a gyrotron) to be able to saturate the electron transitions at high magnetic field; and (*c*) a MAS probe for high resolution that can spin the sample even at cryogenic temperatures. Low temperatures are commonly needed to slow down the electron relaxation—a key factor for high DNP efficiency. Chemists, physicists, and engineers work together in these three directions: introducing new PAs with better performance, building new microwave sources with higher power, and designing MAS probes working at cryogenic temperatures from liquid N_2 and even He. As a result of these tremendous efforts, the number of publications where DNP NMR is employed rises every year.

Three main mechanisms lead to hyperpolarization through DNP in materials: (*a*) solid effect (SE), (*b*) cross effect (CE), and (*c*) Overhauser effect (OE). There is also the thermal mixing mechanism (4), though it is less frequently reported in materials research, and we do not discuss it here. Below we provide brief descriptions of the three main mechanisms. For detailed explanations and quantum mechanical descriptions of the DNP mechanisms, we refer the interested reader, for instance, to the excellent reviews by Corzillius and colleagues (5) and Lafon and colleagues (6).

The SE mechanism requires an unpaired electron and a nucleus coupled by through-space dipolar interaction (7). The polarization transfer relies on the microwave irradiation of the formally forbidden double-quantum (DQ) or zero-quantum (ZQ) transitions at $\omega_e \pm \omega_I$, the sum

or the difference of electron and nuclear Larmor frequencies (see **Figure 1*a***). The microwave irradiation selectively affects the population of the states (e.g., αα and ββ for DQ transition, as shown in **Figure 1*a***), leading to equilibration of the populations. As a result, higher nuclear polarization is generated. The SE is the dominant mechanism when ω_I exceeds the electron paramagnetic resonance (EPR) line width of the unpaired electron. This mechanism was observed for organic radicals with rather narrow EPR lines, for example, 1,3-bis(diphenylene)-2-phenylallyl (BDPA) (8), as well as for paramagnetic metal ions in highly symmetrical environments and with a half-filled electron shell, Mn(II), Gd(III), Cr(III), and Fe(III) (9–14). Recently, SE was also observed with radicals generated by γ-irradiation (15) or present at the surface of the materials due to dangling bonds (16–21).

For the CE mechanism, two unpaired electrons coupled by exchange and/or dipolar interactions and a nucleus interacting with at least one of the electrons are needed (22). In this case polarization is transferred via the 3-spin flip-flop-flip process when microwave irradiation is applied

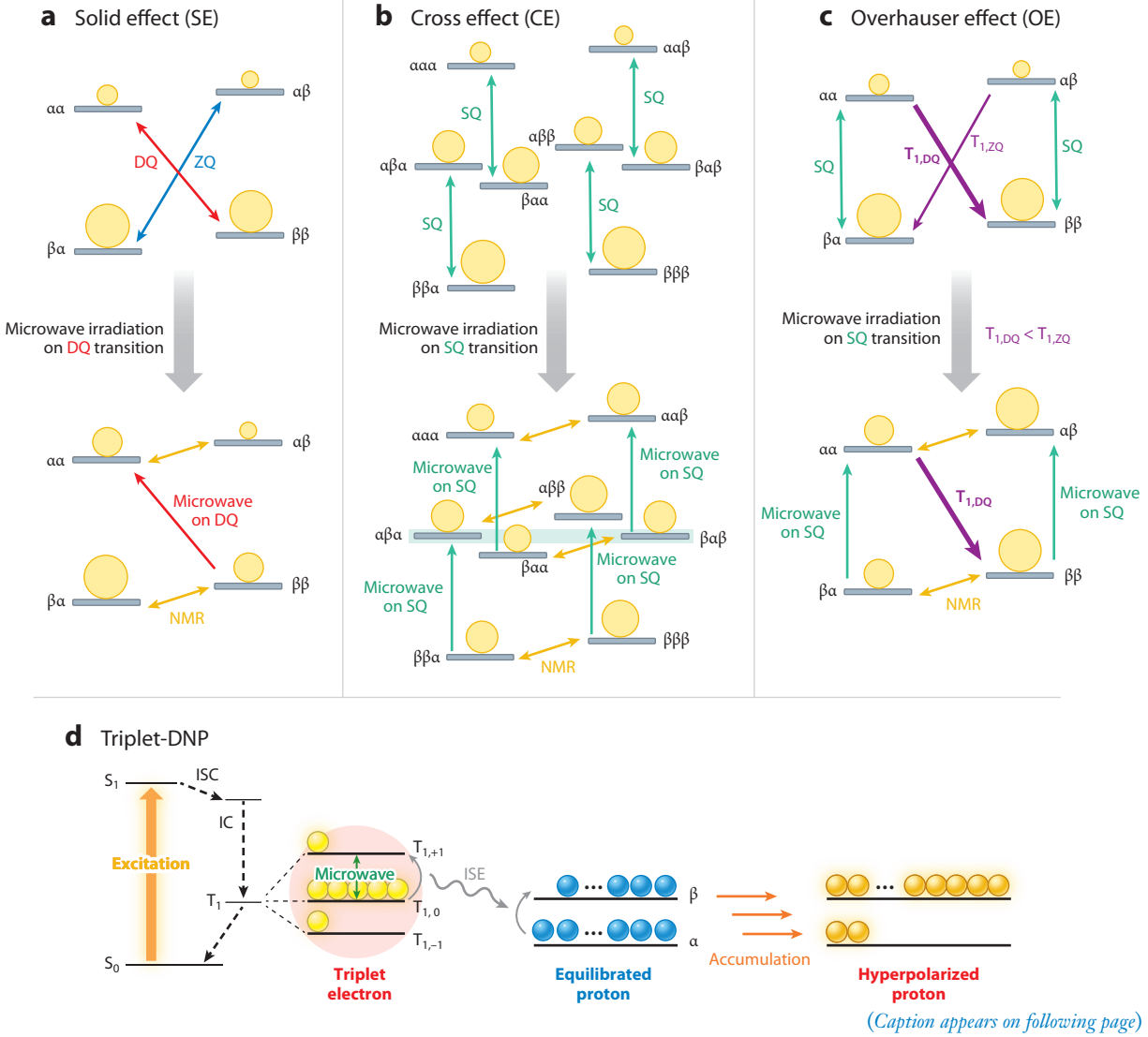

(*Caption appears on following page*)

Figure 1 (*Figure appears on preceding page*)

Schematic representation of the main DNP mechanisms. Populations of the different energy states (*gray bars*) are schematically shown by the size of the orange circles. Hyperpolarized NMR transitions are shown as orange double-headed arrows. Greek symbols α and β refer to electron and nuclear spin states (e.g., αβ denotes a state with electron spin state α and nuclear spin state β). Possible transitions between these states are shown as double arrows (*green*, SQ; *red*, DQ; *blue*, ZQ). Saturation of selected transitions with microwave irradiation is shown as single arrows, pointing in the direction of the increasing population, for simplicity. (*a*) SE: energy level diagram of a two-spin system (electron–nucleus). Microwave irradiation on the DQ (*red arrow*) transitions at $\omega_e - \omega_I$ leads to positive DNP enhancement. Note that the saturation of ZQ transition at $\omega_e + \omega_I$ leads to negative enhancement. (*b*) CE: energy level diagram of a three-spin system (electron 1–electron 2–nucleus). The two green-shaded levels are degenerate when the matching condition $\Delta\omega_e = \omega_I$ is fulfilled. Microwave irradiation at one of the electron's (shown for electron 1) SQ transitions (*green arrows*) leads to nuclear hyperpolarization. (*c*) OE: energy level diagram of a two-spin system (electron–nucleus). Simultaneous microwave irradiation on the SQ transition (*green arrows*) and dominant DQ (or ZQ) cross-relaxation (*purple arrows*; thicker lines indicate more efficient relaxation processes) lead to nuclear hyperpolarization (here again the single arrows are pointing in the direction of increasing population). (*d*) Triplet-DNP: photoexcitation of the PA (*orange arrow*) followed by spin-selective ISC (*black dashed arrow*) creates a large electron spin polarization in the excited state (T_1). The polarization is transferred to protons via the ISE (*wavy arrow*). Panel *d* adapted with permission from Reference 30; copyright 2018 American Chemical Society. Abbreviations: CE, cross effect; DNP, dynamic nuclear polarization; DQ, double quantum; IC, internal conversion; ISC, intersystem crossing; ISE, integrated solid effect; NMR, nuclear magnetic resonance; OE, Overhauser effect; PA, polarizing agent; S, singlet state; SE, solid effect; SQ, single quantum; T, triplet state; ZQ, zero quantum.

on one of the electrons' single-quantum (SQ) transition and the matching condition is fulfilled, namely,

$$\omega_{e1} - \omega_{e2} = \Delta\omega_e = \omega_I, \qquad 2.$$

where the frequency difference of two electrons must be equal to the Larmor frequency of the polarized nucleus (**Figure 1*b***). The matching condition implies that two states in the middle of the energy diagram are degenerate, namely αβα and βαβ (see **Figure 1*b***); hence both have equal populations. This degeneracy, together with the microwave irradiation on the SQ transition of electron 1, results in equal populations of the ββα, αβα, βαβ, and ααβ states. Note that βαα and αββ are not degenerate, and their populations are not equal upon microwave irradiation. Overall, this causes nuclear hyperpolarization—negative in the example shown in **Figure 1*b*** or positive if the SQ transitions of electron 2 are excited with microwave. The CE mechanism is more relevant when the line width of at least one electron is larger than the nuclear Larmor frequency. While it seems to be more demanding in terms of the electron–nuclear system, the CE mechanism relies on allowed SQ transitions; hence it is less demanding in terms of microwave power compared to the SE mechanism. With the development of suitable PAs (e.g., bis-nitroxide radicals) that can fulfill the matching condition, CE became the most efficient mechanism at high-field MAS DNP, surpassing the SE DNP (23–25).

Finally, the OE has been employed for DNP of materials at high field. In contrast to SE and CE, this mechanism is based on cross-relaxation processes (**Figure 1*c***). Simultaneous microwave irradiation of the electron SQ transitions and electron–nucleus cross-relaxation via the dominant DQ (or ZQ) transition provide enhancement of the NMR signal. For cross-relaxation to occur, the electron–nuclear interactions must be stochastically modulated. Cross-relaxation processes are commonly encountered in liquids, where molecular motion modulates the distance between the electron and nucleus, and in conducting solids, through the mobility of the conduction electrons. Nevertheless, the OE was also reported in nonconductive solids (26), though the nature of the modulations in this case is still under debate (26–29). Noteworthily, PAs can in principle be tuned to be more efficient at higher magnetic field by changing the frequency of the modulations (27), though this is not a trivial task. Moreover, in some systems, OE DNP is expected to be efficient even at room temperature; hence, materials can be investigated at conditions relevant for their function. Unfortunately, the occurrence of the OE mechanism is not as general as the SE and CE, and further studies are needed to find suitable materials where it can be efficient.

Besides the mechanisms described above, a conceptually different approach for DNP has recently been suggested. This mechanism was called triplet-DNP as it is based on photoexcited triplet electrons (30). The photoexcitation of a PA by a laser followed by spin-selective intersystem crossing (ISC) produces a large electron spin polarization in the excited triplet state sublevels (**Figure 1*d***). This polarization is then effectively transferred to the nucleus of interest via the integrated solid effect (ISE), an approach for the fast polarization transfer from the short-lived triplet state to the nuclear spins. It allows constructive integration of the negative and positive polarizations of the SE and requires lower microwave power than conventional SE. Another advantage of triplet-DNP is low sensitivity to experimental temperature. Spin-selective ISC allows the creation of high polarization regardless of temperature; hence, it is a very promising tool for materials characterization at working conditions. Note that nuclear spin-lattice relaxation (T_1) of the investigated nuclei should be sufficiently long to enable significant polarization accumulation.

Besides the underlying mechanism, MAS DNP experiments can be classified on the basis of the type of PA as exogenous or endogenous DNP. In the first case, a PA is added to the investigated material right before the NMR experiment. Typically, the PA is dissolved in a solvent containing protons and forms a glass matrix at the temperature of the DNP experiment. The solvent provides high dispersion of the PA molecules and enables good wetting of the sample. Furthermore, it promotes internuclear polarization transfer from the PA through the solvent molecules to the analyte via ^{1}H–^{1}H dipolar coupling (known as spin diffusion). From the solvent to the material, polarization is transferred either via spin diffusion (when protons are present in the material) or via cross-polarization from the solvent protons to the nuclei at the surface of the material. This approach is called DNP surface enhanced NMR spectroscopy (DNP-SENS), as it increases the NMR sensitivity of the nuclei that are close to or at the surface (see Section 3.1 for more details). Organic biradicals operating via the CE mechanism are the most efficient exogenous PAs to date.

In endogenous DNP, PAs are introduced during the synthesis of a material or via postsynthetic modifications. The PA is distributed throughout the material and can (*a*) directly polarize nuclei coupled to the PA and (*b*) indirectly polarize more distant nuclei via spin diffusion if the later process occurs efficiently in the material. Endogenous DNP is not surface-selective but helps to avoid contact between the reactive surfaces and the PA solution. DNP from endogenous PAs occurs predominantly via SE or, in the case of conduction electrons, via OE. Above a certain concentration of the PAs, the CE mechanism may become possible too; however, it is assumed to not be efficient (14).

Overall, DNP can be performed via several different mechanisms depending on the material studied, the PA chosen, and the experimental conditions used. Each mechanism provides different benefits and has its own limitations. In what follows, we discuss what information can be obtained by careful design of the DNP experiment and proper choice of the PA formulation. We highlight the main achievements of high-field MAS DNP NMR in materials characterization and structure our discussion on the basis of the type of material.

3. DNP APPLICATIONS IN MATERIALS SCIENCE

The versatility of high-field MAS NMR coupled with the improved sensitivity provided by DNP allows answering various questions in materials research that could not be addressed by other techniques or by conventional solid-state NMR spectroscopy. In this section, different types of materials and cases are presented where DNP-enhanced NMR becomes a panacea for addressing the research question. The examples were chosen in an effort to represent most of the systems studied to date and are summarized in **Table 1**.

Table 1 Application of DNP solid-state NMR spectroscopy in materials research

Material system	Nuclei	Challenge(s)[a]	Approach(es)[b]	Fundamental insights
Surfaces and interfaces: catalysts (Section 3.1)				
Sn-zeolite catalysts (36, 95–97)	^{119}Sn	Low quantity, low NA, broadening due to large CSA	DNP-SENS via TEKPol	Active site structure and position in zeolite
Pt/SiO_2 (39)	^{195}Pt	Broadening due to large CSA	DNP-SENS via TEKPol	Local structure of Pt sites
Surface organometallic chemistry catalysts (38, 40, 42, 54, 56–58)	^{13}C	Low NA	DNP-SENS via TEKPol	Local structure Mechanism of grafting
	^{15}N	Low NA, low γ_I	DNP-SENS via TEKPol	
	^{17}O	Low NA, quadrupolar broadening	DNP-SENS via TEKPol/ TOTAPOL	
	^{15}N	Low NA, low γ_I		
Nitridated SiO_2 (59)	^{15}N	Low NA, low γ_I	DNP-SENS via bTbK	Structure-activity relationship
$Ca_3Al_2O_6$ for CO_2 capture (60)	^{27}Al	Quadrupolar broadening	DNP-SENS via TEKPol	Deactivation mechanism
Surfaces and interfaces: catalyst support (Section 3.1)				
Acidic supports: SiO_2, Al_2O_3, amorphous silica-aluminas (43–47, 49, 61–64)	^{27}Al	Quadrupolar broadening, 2D correlation is needed to improve resolution	DNP-SENS via TEKPol/ TOTAPOL/bTbK	Discrimination of surface sites Spatial proximities and connectivity
	^{29}Si	Low NA		
	^{17}O	Broadening due to large CSA, quadrupolar broadening	DNP-SENS via TEKPol/bTbK	Surface site structure Measurement of O–H distances
	^{15}N	Low NA, low γ_I	DNP-SENS via TEKPol	Surface acidic sites via pyridine adsorption
CeO_2 (48)	^{17}O	Quadrupolar broadening	DNP-SENS via TEKPol	Distinguishing of first three surface layers
Surfaces and interfaces: reaction intermediates (Section 3.1)				
Single-site catalysts and NPs (38, 50, 51)	^{13}C	Low quantity, low NA	DNP-SENS via TEKPol/AMUPol	Mechanistic studies Surface intermediates
Surfaces and interfaces: batteries (Section 3.1)				
Anodes (65, 66, 70)	^{13}C	Low NA	DNP-SENS via TEKPol	Structure of SEI Composition of SEI-anode interface Structure of SEI at ambient T
	^{7}Li, ^{19}F	Selectivity of enhancement	Endogenous DNP via Li dendrides, OE	
Cathodes (67)	^{13}C	Low NA	DNP-SENS via TEKPol	Composition of CEI
Coatings (68, 69)	^{29}Si, ^{13}C	Low NA	DNP-SENS via TEKPol/ MIDNP via Fe(III)	Composition and structure of coatings
Surfaces and interfaces: QDs (Section 3.1)				
QDs (78–81)	^{133}Cs	Quadrupolar broadening	DNP-SENS via TEKPol/ AMUPol	Surface versus bulk sites Location of Cd(II) dopant in InP
	^{77}Se, ^{125}Te	Broadening due to large CSA, low γ_I		
	^{113}Cd	Broadening due to large CSA, inhomogeneous broadening		

(*Continued*)

Table 1 (*Continued*)

Material system	Nuclei	Challenge(s)[a]	Approach(es)[b]	Fundamental insights
Surfaces and interfaces: miscellaneous (Section 3.1)				
Biomaterials (18, 71, 72, 75–77)	^{29}Si	Low NA, 2D correlation is needed to improve resolution	DNP-SENS via TEKPol/AMUPol/bCTbK	Structure of surface functionalities Adsorbate structure, location, and interactions Bulk versus surface sites Binding sites of peptides
	^{43}Ca	Low γ_I, quadrupolar broadening		
	^{15}N	Low NA, low γ_I		
Membranes (73)	^{13}C	Low quantity, low NA	DNP-SENS via AMUPol	Surface functionalities
Cements (74)	^{29}Si	Low NA	DNP-SENS via AMUPol	3D structure
Porous materials: mesopores (Section 3.2)				
MCM-41, SBA-15, PMOs (25, 31, 82, 84–87)	^{13}C	Low quantity, low NA	DNP-SENS via TEKPol/bTbK/AMUPol	Structure of functionalities Interconversion of functionalities Spatial distribution Assessment of functionalization approach
	^{15}N	Low NA, low γ_I		
	^{29}Si	Low NA	Solvent free, via grafted nitroxides, CE	Structure of functionalities
Supported catalytic sites (33, 41, 57, 83, 88–89)	^{29}Si	Low NA, 2D correlation is needed to improve resolution	DNP-SENS via TEKPol/AMUPol/bCTbK/TEMPO	Structure of supported active sites
	^{15}N	Low NA, low γ_I		
	^{27}Al	Quadrupolar broadening		
HYPSO (90–94)	Not applicable	PA-analyte separation	Solvent free, via grafted nitroxides, CE	Polarization of guest molecules
Porous materials: micropores (Section 3.2)				
P-modified Zeosils (98)	^{31}P	Low quantity	DNP-SENS via TEKPol	Nature of catalytic active sites
MFI nanosheets (99)	^{29}Si	Low NA, 2D correlation is needed to improve resolution	DNP-SENS via TEKPol	Crystallization mechanism
Catalyst intermediates (100, 101)	^{13}C	Low quantity, low NA	DNP-SENS via TEKPol/bTbK	Mechanism of deactivation
MOFs (103–105)	^{15}N	Low NA, low γ_I	DNP-SENS via TEKPol/bTbK/AMUPol	Structure of surface functionalities
MIL-100(Al) (102)	^{27}Al	Quadrupolar broadening	DNP-SENS via TOTAPOL	Metal-linker proximities
UiO-66, MOF-253 (106)	^{195}Pt	Broadening due to large CSA	DNP-SENS via TEKPol	Geometry of Pt(II) sites
MIP-206 (107)	^{17}O	Low NA	DNP-SENS via AMUPol	Structure at natural abundance of ^{17}O

(*Continued*)

Table 1 (*Continued*)

Material system	Nuclei	Challenge(s)[a]	Approach(es)[b]	Fundamental insights
Bulk inorganic materials (Section 3.3)				
Oxides (108–110)	Not applicable	Slow spin diffusion	Pulse-cooling with TEKPol	Hyperpolarization of bulk nuclei
Silicon NPs, diamonds, fused quartz (15–21, 111–113)	^{29}Si/^{13}C	Low NA, reactive surfaces	Endogenous DNP via dangling bonds, SE	Characterization of NPs or liquids around
$Li_4Ti_5O_{12}$ electrode (12, 13)	^{17}O, ^{6}Li	Low NA, quadrupolar broadening	MIDNP, Mn(II) MIDNP, Fe(III)	Structure of electrode material Role of Fe(III) in electrochemistry
Y-doped CeO_2 (119)	^{89}Y	Low γ_I	MIDNP, Gd(III)	Oxygen vacancies distribution
Polymers (Section 3.4)				
Synthetic polymers (121–123)	^{13}C	Low quantity, low NA	Film casting with TOTAPOL or bCTbK/IWI with bis-nitroxides	Chain-terminal groups/diluted monomers
	^{15}N	Low NA, low γ_I		
Thin films (124)	^{13}C	Low quantity	IWI with bis-nitroxides	Stacking arrangement
Pharmaceuticals and composites (Section 3.5)				
APIs and dosage forms (129–138)	^{13}C	Low NA	IWI with bis-nitroxides/hot-melt extrusion or spray-drying with TOTAPOL or AMUPol	Structure and domain size of APIs API–excipient interactions Impurity phases
	^{15}N	Low NA, low γ_I		
	^{35}Cl	Low quantity, broadening due to large CSA, quadrupolar broadening	IWI with bis-nitroxides	Structure of Cl^--based APIs General strategy for DNP of fluorine-APIs Room temperature and high-field DNP NMR
	^{19}F	Formulation	IWI with bis-nitroxides	
	^{13}C	Low NA	IWI with bis-nitroxides, OE	

Abbreviations: API, active pharmaceutical ingredient; CE, cross effect; CEI, cathode electrolyte interphase; CSA, chemical shift anisotropy; DNP, dynamic nuclear polarization; HYPSO, hyperpolarizing solids; IWI, incipient wetness impregnation; MIDNP, metal-ion DNP; MOF, metal-organic framework; NA, natural abundance; NMR, nuclear magnetic resonance; NPs, nanoparticles; OE, Overhauser effect; PA, polarizing agent; PMOs, periodic mesoporous organosilicates; QDs, quantum dots; SE, solid effect; SEI, solid electrolyte interphase; SENS, surface enhanced NMR spectroscopy; γ_I, gyromagnetic ratio for the isotope.

[a]Experimental challenges hindering the application of conventional solid-state NMR.

[b]Type of DNP approach including the PA. The DNP mechanism is indicated if it was investigated. For MIDNP, the PA is mentioned, while the proposed DNP mechanism (SE) is omitted.

3.1. Surfaces and Interfaces

Often it is the surface or the interface between two phases that leads to the unique properties of a material. For example, in heterogeneous catalysis the chemical transformations occur at the surface of the catalyst where the so-called active sites are present. In rechargeable batteries, performance depends on not only the bulk of the cathode and anode materials but also on the electrode/electrolyte interface. Surfaces and interfaces are also investigated when the chemistry of coatings or biocompatible materials is to be understood. Finally, the optical properties of quantum dots (QDs)—colloidal nanocrystals terminated by surfactant molecules—strongly depend on the electronic structure of surface atoms: The undercoordinated surface atoms cause localized electronic states that reduce photoluminescence quantum yields.

When characterizing surface/interface atoms, the inherently low sensitivity of NMR is amplified by the extremely small number of surface atoms as compared to the bulk ones, making it very challenging to collect informative spectra. For characterizing surface species, Emsley, Lesage, Copéret, Rossini, and coworkers developed DNP-SENS (31, 32). In DNP-SENS, an analyte is impregnated with just enough radical solution, typically nitroxide biradicals, to uniformly wet the surface of the material. Polarization is then transferred to the nuclei at the surface of the sample either directly or indirectly through the frozen solvent molecules (**Figure 2**). Due to the

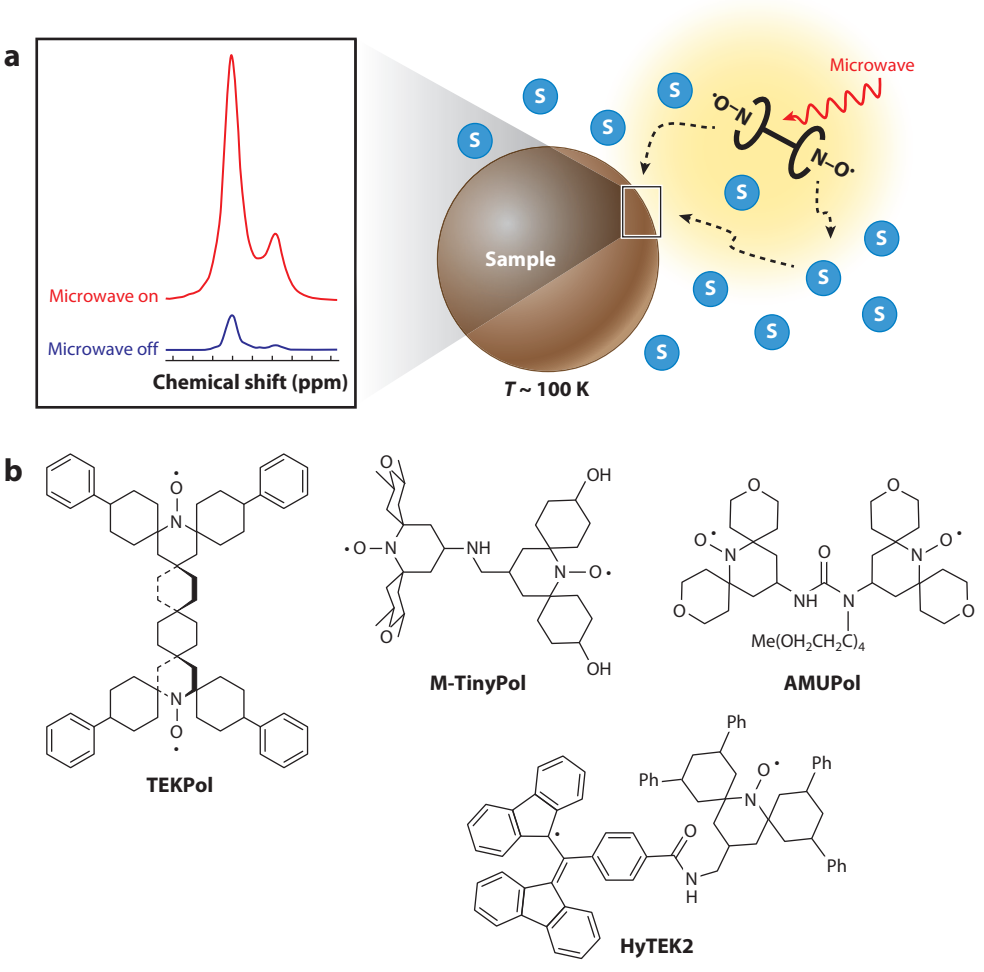

Figure 2

(*a*) An illustration of the concept of DNP-SENS. Microwave irradiation (*red arrow*) of the bis-nitroxide radical (backbone structure of the radical schematically represented as *black circles*), dissolved in the frozen (at approximately 100 K) solvent (*blue circles*), leads to polarization transfer (within the region highlighted in *yellow* and indicated by *black dashed arrows*) directly to the nuclei at the surface of the material or via solvent molecules resulting in enhancement of the NMR signal (*red spectrum*). (*b*) Bis-nitroxide and mixed BDPA-nitroxide biradicals reported in literature as PAs for DNP-SENS (25, 33–35). Note that the operating mechanism for these PAs is CE. Abbreviations: BDPA, 1,3-bis(diphenylene)-2-phenylallyl; CE, cross effect; DNP, dynamic nuclear polarization; NMR, nuclear magnetic resonance; PA, polarizing agent; SENS, surface enhanced NMR spectroscopy.

proximity to the PAs, surface atoms build up hyperpolarization faster than the bulk and their spectral contribution is therefore enhanced. The technique thus highlights the signals from the surface and subsurface atoms.

In heterogeneous catalysis research, DNP-SENS has been utilized to study (*a*) the active site structure (36–42); (*b*) the surface of the support, a high-surface-area compound used to disperse the active sites (43–49); and (*c*) adsorbed reactants and intermediates of chemical transformations (38, 50, 51). For instance, Wolf et al. (36) exploited DNP enhancement to characterize tin active sites in Sn-β zeolites with only a few wt% of tin, a Lewis acid catalyst for upgrading cellulose-based renewable feedstocks. ^{119}Sn nuclei exhibit large chemical shift anisotropy (CSA), which broadens the NMR signal (>200 ppm span), and have a rather low natural abundance (NA) (8.59%), thus leading to very long acquisition times: between 14 and 60 h for a 1D NMR spectrum. DNP-SENS enabled rapid acquisition (<1 h) of high-quality ^{1}H–^{119}Sn cross-polarization (CP) MAS spectra of Sn zeolites without ^{119}Sn enrichment. Moreover, high enhancement (greater than 60) allowed researchers to record cross-polarization magic-angle turning (CPMAT) spectra and to measure the CSA parameters for each ^{119}Sn site. These NMR signatures were assigned to the specific molecular structures of Sn sites with the assistance of computational chemistry. Recently, Venkatesh et al. (39) applied DNP-SENS to Pt single sites dispersed on amorphous SiO_2, a model system for supported Pt catalysts. Although ^{195}Pt solid-state NMR signals are severely broadened by CSA (>8,000 ppm span), the ^{195}Pt spectrum was obtained with sufficient SNR for a static sample (**Figure 3*a***). Combined with fast MAS proton-detected NMR and augmented by DFT studies, these experiments enabled determination of the Pt local structure.

DNP-SENS has become an indispensable characterization tool for the groups focusing on surface organometallic chemistry (SOMC) (52, 53), a synthetic approach toward well-defined supported catalysts. Typically, an organometallic precursor containing alkyl, alkoxy, amide, or other ligands is grafted on the surface of an oxide support. DNP-SENS can be used to monitor the grafting process. It enabled the fast detection of ^{13}C (only 1% NA) (38, 42, 54–56) and ^{15}N (low NA and low γ) (56, 57) NMR spectra, thereby providing information about the chemical environment of the metal ions on the surface. Perras et al. (40) and Gutmann et al. (58) have demonstrated that MAS NMR assisted by DNP is able to differentiate between metal-support link atoms and nonbinding atoms of the support. This helped researchers to understand the mechanism of grafting and to locate the grafted sites. The changes on the microscopic level in the structure of surface sites revealed by DNP-SENS can be correlated with the performance of the materials. For instance, Thankamony et al. (59) provided an explanation for a decrease in the catalytic activity of nitridated fibrous nanosilica used as a solid base catalyst when higher nitridation temperature is used: Elevated temperature facilitates the conversion of primary silylamine sites into secondary ones, as was found in the ^{15}N DNP-SENS experiments. Kim et al. (60) monitored the structure of Al sites on calcium-aluminum mixed oxides upon CO_2 capture and sorbent regeneration cycles. Combination of X-ray diffraction (XRD) and DNP-SENS of the quadrupolar ^{27}Al nuclei (**Figure 3*b***) revealed that $Ca_3Al_2O_6$ transformation to $Ca_{12}Al_{14}O_{33}$, followed by segregation of the Al_2O_3 phase, leads to thermal sintering of the sorbent particles and results in reduced CO_2 uptake.

Surface properties of the catalysts' support (metal oxides, carbon materials, etc.), such as composition, acidity/basicity, and structure of surface sites, can play a significant role in the catalytic performance. DNP-SENS has been applied to probe the surface sites of different oxide supports by enhancing the NMR signal both of the support itself (44, 47–49, 61–63) and of the probe molecules for evaluation of surface acidity (43). Owing to the 20-times enhancement achieved by DNP-SENS, 2D ^{27}Al multiple-quantum (MQ) MAS and ^{27}Al homonuclear dipolar-mediated correlation experiments could be performed for γ-Al_2O_3 within <7 h (49). The obtained spectra

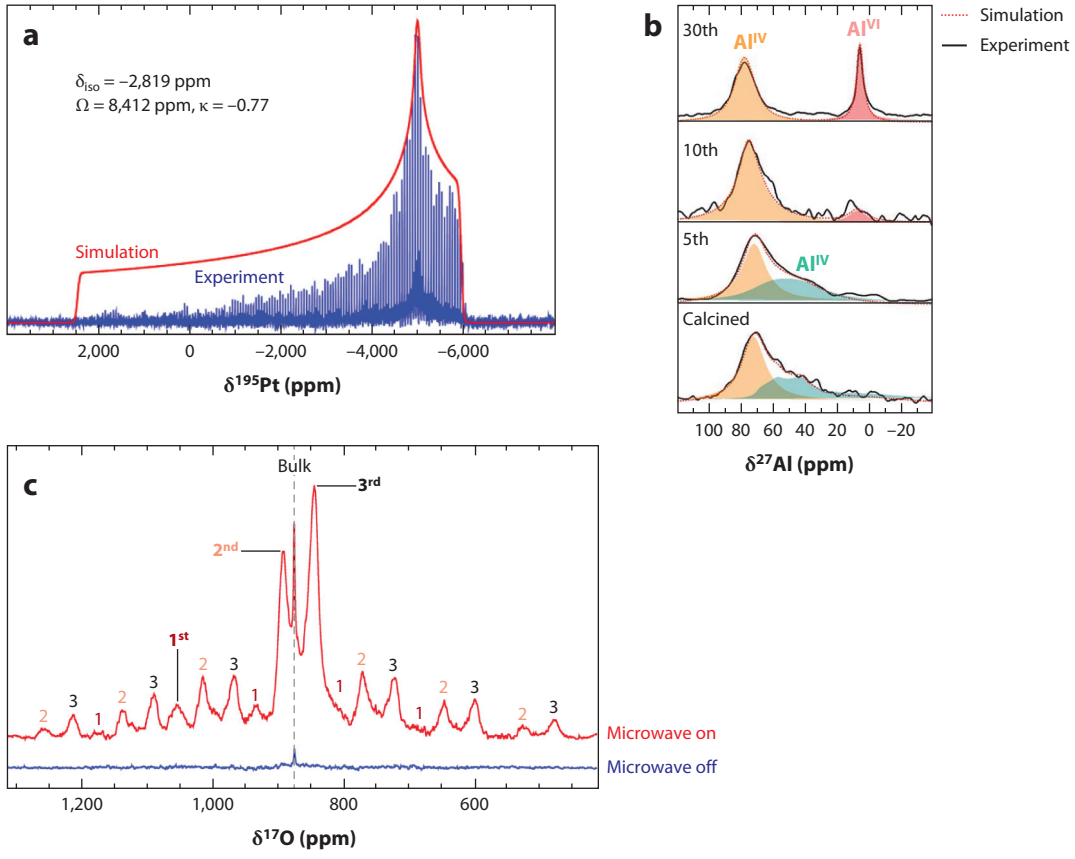

Figure 3

DNP-enhanced NMR for characterization of surfaces and interfaces. (*a*) Ultra wideline static ^{1}H–^{195}Pt BRAIN-CP-WCPMG spectrum of supported active site 1@SiO_2 at 9.4 T and 105 K, where 1 = [Pt(OSi(O^{t}Bu)$_3$)$_2$(COD)]. Panel *a* adapted with permission from Reference 39; copyright 2020 American Chemical Society. (*b*) Monitoring of the interconversion of Al surface sites for $Ca_3Al_2O_6$-stabilized CaO sorbent with ^{27}Al DNP-SENS after 5, 10, and 30 cycles of CO_2 capture and regeneration. Spectra were recorded at 14.1 T and 100 K. Panel *b* adapted with permission from Reference 60; copyright 2018 American Chemical Society. (*c*) Discrimination of the first three surface layers of CeO_2 with direct ^{17}O DNP (14.1 T). The red spectrum was recorded with microwave on and the blue was recorded with microwave off. Labels 1, 2, and 3 of the signals and sidebands correspond to the subsurface layers from which they arise. Panel *c* adapted with permission from Reference 48; copyright 2017 The Royal Society of Chemistry. Abbreviations: DNP, dynamic nuclear polarization; NMR, nuclear magnetic resonance; SENS, surface enhanced NMR spectroscopy.

helped to distinguish Al sites and resolve relative spatial proximities between different Al sites. Direct polarization transfer from PAs to ^{17}O nuclei allowed researchers to distinguish the first three surface layers of CeO_2 with high selectivity (**Figure 3*c***) (48). These results are of great interest because the signals of (sub)-surface layers can be used to distinguish between various morphologies of ceria. DNP-enhanced ^{17}O NMR was utilized to characterize the surface sites of γ-Al_2O_3, SiO_2, and mixed silica-alumina oxide. It allowed the identification of different bare oxygen and hydroxyl groups on γ-Al_2O_3 (47). Moreover, it was even possible to measure the O–H bond length on various supports with subpicometer precision, that is, to probe the strength of Brønsted acidity (64). Finally, MAS DNP NMR can provide detailed structural information on the interface in mixed oxide supports, such as silicated alumina or aluminosilicate (45, 46).

For example, Valla et al. (45) demonstrated that Si and Al precursors are preferentially grafted in Si(IV)-to-Al(IV) fashion and proposed that this specific interface connectivity enables the formation of strong Brønsted acid sites.

DNP enhancement is useful for detecting and analyzing reaction intermediates adsorbed on the catalysts (38, 50, 51). Using ^{13}C DNP-SENS and 2D ^{13}C–^{13}C correlation spectroscopy, Ong et al. (38) characterized the key intermediates that are responsible for catalytic activity and deactivation of tungsten-based catalysts for olefin metathesis. Enhancement factors of up to 170 enabled investigating the surface species upon CO oxidation on supported Pt nanoparticles (NPs), alleviating the need for ^{13}C-labeled reactants (51).

High-field MAS DNP greatly benefits investigations of the surface chemistry of electrode materials, which play an important role in the battery's performance. Since the report by Leskes et al. (65) where DNP-SENS ^{13}C CPMAS spectra were recorded to characterize the solid electrolyte interphase (SEI) layer, this approach has been increasingly applied in the study of battery materials. It allowed researchers to reveal the structure of the SEI (65, 66) and the cathode electrolyte interphase (CEI) (67) and to monitor their structural changes following battery cycling (**Figure 4*a***). Thin protection coatings for cathode materials have also been studied by MAS DNP NMR (68, 69). Moreover, DNP-enhanced NMR can be used to probe the interfacial region between the SEI and the anode surface, revealing the covalent network between them (66).

DNP-SENS is not the only approach that can be applied for studying interfaces in batteries. Noteworthily, Hope et al. (70) demonstrated that MAS DNP NMR can be performed even at room temperature by exploiting conduction electrons of lithium metal present in batteries (endogenous DNP via OE mechanism). Thus, batteries can potentially be studied without affecting the surface with exogenous PAs. Moreover, appreciable enhancements were achieved under static conditions, suggesting that the OE DNP approach can be extended to in situ experiments in order to monitor Li dendrite growth or SEI structural changes upon charge/discharge. In our research group, we are developing additional endogenous DNP formulations for NMR studies of battery materials (for more details, see Section 3.3). For example, Haber et al. (69) introduced Fe(III) dopants into the bulk of coated particles and revealed the interphase structure between the coating and the electrode material. Furthermore, a combination of the exogenous and endogenous DNP approaches was shown to be a promising structural tool for interfaces. In the case of thin coatings, comparison of spectra enhanced through nitroxides (DNP-SENS) and Fe(III) provided insight into the architecture of the thin coating (**Figure 4*b***).

Nevertheless, due to its high sensitivity and generality, DNP-SENS is still the most used method for characterization of surfaces. DNP-SENS is a powerful tool to decipher the network of surface functionalities (71), assess interactions of dilute organic molecules on the surface (72), characterize coatings for membranes (73), determine the composition of cement (74), and study surfaces/interfaces in biomaterials research (18, 75–77). For instance, unreceptive ^{43}Ca nuclei (low γ and spin 7/2), an important element in biomaterials, can be detected at natural abundance, providing the unambiguous discrimination of core and surface calcium atoms in hydroxyapatite NPs (75).

Finally, the Kovalenko research group introduced DNP-SENS to QDs research (78). They recorded 1D spectra of ^{31}P, ^{77}Se, ^{113}Cd, ^{125}Te, and ^{133}Cs nuclei for common QD materials, such as CdSe, CdTe, InP, PbSe, PbTe, and $CsPbBr_3$, that were stabilized by various capping ligands and dispersed in suitable solvents. These experiments allowed the researchers to distinguish surface and bulk atoms in QDs (78, 79). Noteworthily, previously inaccessible 2D correlation experiments (^{13}C–^{113}Cd, ^{31}P–^{113}Cd, ^{77}Se–^{113}Cd) can be readily performed with DNP on QDs, elucidating the bonding motifs between the QD surface and the capping ligands (78), revealing the surface stoichiometry (80), or locating the Cd(II) ions in Cd-doped InP QDs (81).

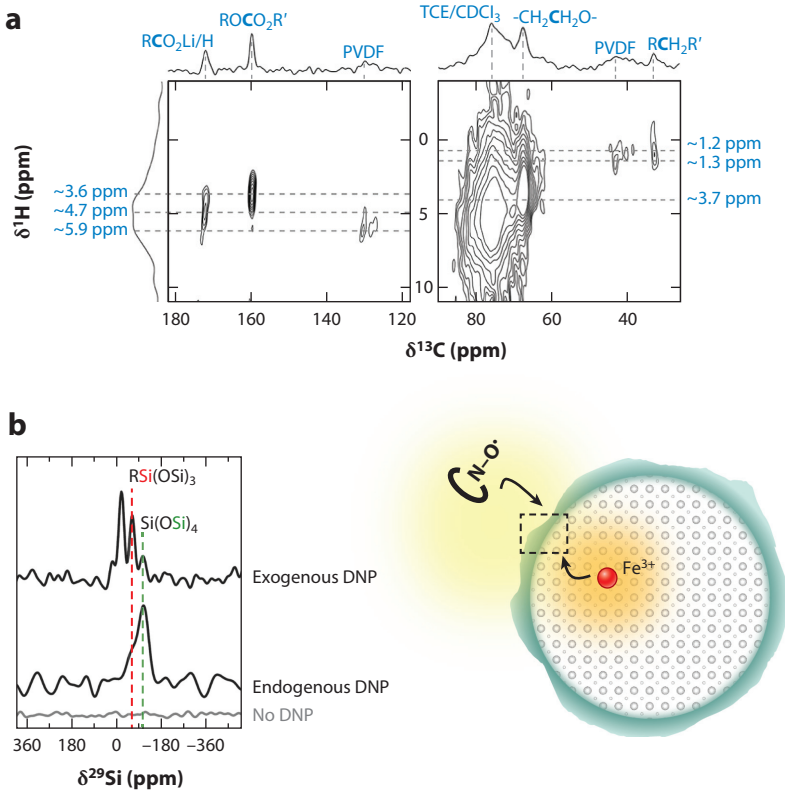

Figure 4

MAS DNP NMR studies of battery materials. (*a*) Characterization of the CEI formed on the Li_2RuO_3 cathode after a single charge/discharge cycle with 2D HETCOR DNP NMR. Panel *a* adapted with permission from Reference 67; copyright 2020 Hestenes, Ells, Navarro Goldaraz, Sergeyev, Itin, and Marbella (CC BY 4.0) (*b*) Revealing the interface structure between electrode material and the coating by applying a combination of exogenous DNP with nitroxide radical and endogenous DNP with Fe(III) dopant as a PA. Panel *b* adapted with permission from Reference 69; copyright 2021 American Chemical Society. Abbreviations: CEI, cathode electrolyte interphase; DNP, dynamic nuclear polarization; HETCOR, heteronuclear correlation; MAS, magic angle spinning; NMR, nuclear magnetic resonance; PA, polarizing agent.

3.2. Porous Materials

Another class of materials that benefit from MAS DNP are materials containing pores of different size. This includes mesoporous materials, such as MCM-41, SBA-15, periodic mesoporous organosilicates (PMOs), and ordered mesoporous carbon (OMC), as well as microporous zeolites and metal-organic frameworks (MOFs). Porous materials are important for catalysis, gas separation and storage, drug delivery, and adsorption. Hence, they are of great interest and can be efficiently probed through MAS NMR equipped with sensitivity from DNP.

Mesoporous materials contain pores with diameters between 2 and 50 nm; hence some exogenous PAs can be accommodated inside the pores, unless these host other molecules inside. The surface-to-bulk ratio in mesoporous materials is very high ($S_{BET} > 600$ m^2/g). Therefore, the DNP-SENS approach is extremely suitable for these materials. The majority of the reports on mesoporous materials are dedicated to the characterization of surface organic functionalities:

structure analysis (25, 31, 82, 83), monitoring interconversion (25), control of spatial distribution (**Figure 5*a***) (84–86), and assessment of different approaches for surface functionalization (e.g., co-condensation versus postsynthesis grafting) (84, 86). Typically, samples are prepared by incipient wetness impregnation (IWI) of the solution of the PAs into the pores of the analyte for characterization through the DNP-SENS approach. However, in a recent report, de Oliveira et al. (82) suggested a new strategy for solvent-free DNP that circumvents the possible effect of solvent molecules on surface functionalities. Moreover, it was demonstrated that PAs do not necessarily have to fit inside the pores (87). When the pores were occupied by guest molecules (e.g., surfactant), sufficient signal enhancements were observed for the surface functionalities despite several hundred nanometers separating the target species from the PA that was outside of the pores. This was explained by hyperpolarization transfer via ^{1}H–^{1}H spin diffusion.

In addition to organic functionalities, mesoporous materials can support catalytically relevant species such as organometallic complexes (33, 57, 83), Lewis acidic Al sites (88), acid-base pairs (41), or metal NPs (89). In these cases DNP-enhanced NMR is a vigorous tool for understanding these species' local structure and performance. For example, multinuclear 1D and 2D NMR analysis of the phenylpyridine (ppy)-PMO material before and after functionalization with an iridium complex allowed researchers to distinguish the outer and inner layers of ppy moieties, determine their fraction, and show that only outer moieties are accessible for Ir complexes (approximately one-third of the surface sites) (83). This analysis was only possible thanks to sensitivity enhancement from DNP.

Interestingly, mesoporous materials not only are targets for DNP NMR studies, but also play the role of a matrix for the PAs (90–94). For that, radicals are chemically attached to the surface of mesoporous silica, and such materials are called hyper polarizing solids (HYPSOs). They can hyperpolarize condensed gases in their pores, including hydrocarbons, an approach that is very promising for mechanistic studies of catalytic transformations in mesoporous materials (93).

In contrast to mesoporous materials, microporous ones contain pores of less than 2 nm diameter. Hence, standard PAs used for DNP-SENS do not fit inside the pores. Nevertheless, there are a few examples where MAS DNP NMR studies with exogenous radicals were performed on microporous materials, namely zeolites and MOFs. In this case, polarization is transferred to the target nuclei via spin diffusion. As was discussed in Section 3.1, DNP-enhanced MAS NMR helped to reveal the structure of active Sn sites in the tin-containing zeolites BEA and CHA (36, 95–97) and identify the sites' position within the zeolite framework (**Figure 5*b***) (96). Studies through receptive nuclei such as ^{31}P can also benefit from DNP. For example, DNP provided the sensitivity necessary to carry out ^{29}Si-filtered ^{31}P detection and ^{31}P–^{31}P 2D correlation experiments that allowed distinguishing sites with P–O–Si and P–O–P linkages in phosphorus-modified siliceous zeolites, which are catalysts for selective dehydration of biomass derivatives (98). Another striking example of DNP application is the mechanistic study of the crystallization of mesostructured MFI zeolite nanosheets. The 2D ^{29}Si–^{29}Si J-mediated NMR enabled by DNP provided evidence for transformation of initially formed nanolayered silicates into the final mesostructured product (**Figure 5*c***) (99). This analysis was used to establish the covalent connectivity between two phases supporting the previously unknown mechanism of crystallization. Finally, the advantage of the high sensitivity of MAS DNP NMR has been exploited to detect minute quantities of hydrocarbon intermediates of catalytic transformations present inside zeolite pores (100, 101). The structure and interactions of these intermediates with the surface sites of the zeolites was probed by 2D J- and D-mediated correlation experiments (100). This provided insights into catalyst deactivation.

MOFs are another class of microporous materials, which makes them well suited for various applications from gas storage to heterogeneous catalysis. However, in contrast to zeolites, their

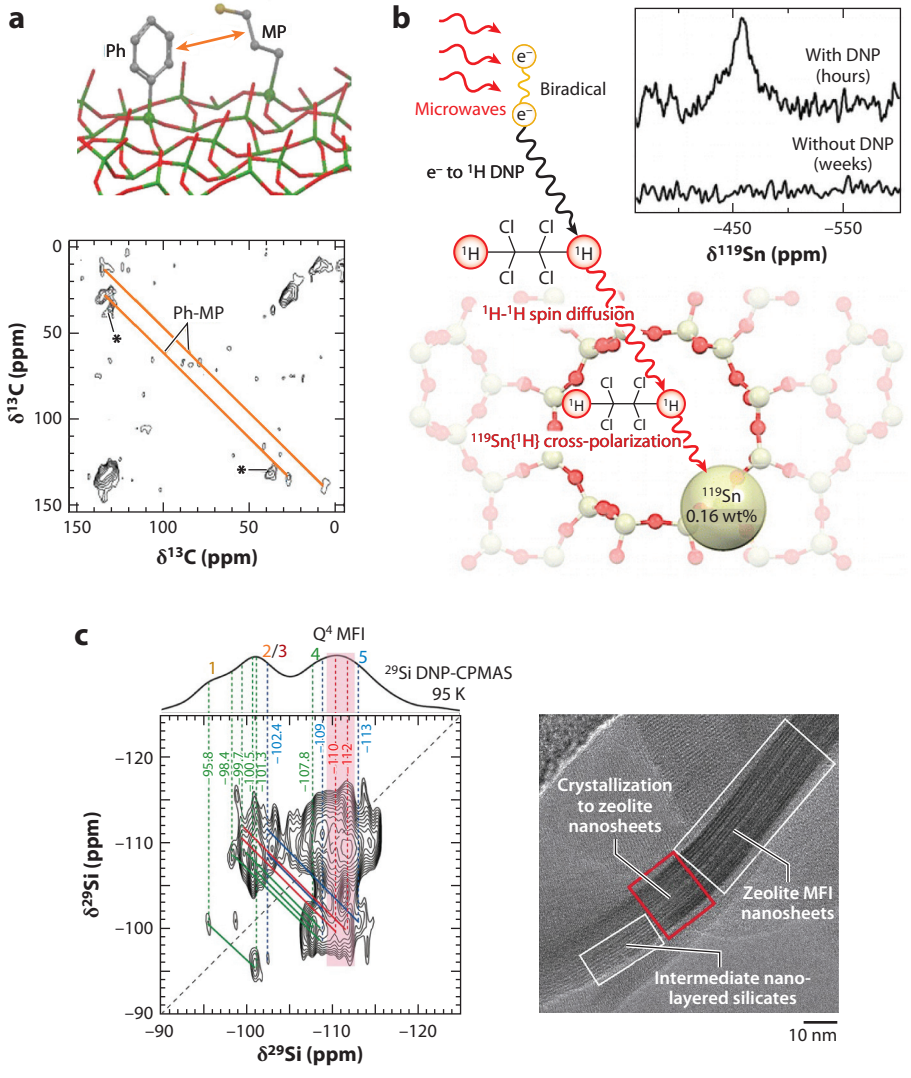

Figure 5

Application of DNP NMR to porous materials. (*a*) Determination of the spatial distribution between Ph and MP functionalities on mesoporous silica by means of DNP-enhanced 2D ^{13}C–^{13}C homonuclear correlation at natural abundance. Panel *a* adapted with permission from Reference 85; copyright 2017 American Chemical Society. (*b*) ^{119}Sn DNP-SENS of tin sites in zeolite Sn-BEA at natural abundance and low wt%. Polarization is transferred from the PA to ^{119}Sn nuclei inside micropores via ^{1}H–^{1}H spin diffusion assisted by solvent molecules. Panel *b* adapted with permission from Reference 95; copyright 2014 American Chemical Society. (*c*) Mechanistic studies on zeolite MFI crystallization: 2D J-mediated $^{29}Si\{^{29}Si\}$ correlation spectrum and TEM image support transformation of layered silicates into mesostructured MFI. Panel *c* adapted with permission from Reference 99; copyright 2017 Wiley-VCH. Abbreviations: CPMAS, cross-polarization magic angle spinning; DNP, dynamic nuclear polarization; MP, mercaptopropyl; NMR, nuclear magnetic resonance; PA, polarizing agent; Ph, phenyl; SENS, surface enhanced NMR spectroscopy; TEM, transmission electron microscopy.

framework is less rigid; hence, some of the exogenous PAs can diffuse inside the pores (102). Similar to its use for mesoporous materials, DNP-enhanced solid-state NMR has been utilized to characterize surface functionalities in MOFs—nitrogen-containing ligands for metal binding (103, 104) or peptides (105)—and probe their interactions with the surface of the MOF. Moreover, MAS DNP NMR has enabled researchers to perform very challenging experiments, such as implementation of highly insensitive ^{27}Al–^{13}C 2D correlations for Al-based MIL-100 (102), acquisition of a 10,000 ppm ultra wideline ^{195}Pt NMR spectrum of Pt sites present in UiO-66 and MOF-253 (106), and detection of quadrupolar-broadened ^{17}O spectra at 0.037% NA for metal-oxo clusters that are nodes of MIP-206 (107). These experiments provided important structural information on the porous frameworks that can be extended to other framework types. Therefore, DNP NMR is a good complementary tool for XRD to elucidate the structure of MOFs, especially on the atomic scale.

3.3. Bulk Inorganic Materials

Macroscopic properties of inorganic materials—oxides, silicates, phosphates, aluminates, ceramics, etc.—are often defined by their bulk structure. Solid-state NMR is a good complementary tool for diffraction techniques, especially in cases where the inorganic solids have some degree of disorder. However, inorganic materials often contain nuclei with low receptivity and/or low NA, making hyperpolarization in the bulk desirable in such cases. Nevertheless, this is not straightforward, as the bulk nuclei are far away from the surface and thus cannot be polarized by DNP-SENS (see Section 3.1). These materials do not contain high-γ ^{1}H nuclei in the bulk (in contrast to organic materials) that are known to efficiently transfer the polarization through the sample. Therefore, other sources of polarization and other routes for polarization transfer have been suggested in recent years.

Björgvinsdóttir et al. (108–110) have demonstrated that nuclei with moderate NA and γ, such as ^{6}Li, ^{29}Si, ^{113}Cd, and ^{119}Sn, can also transfer polarization to the bulk of the materials. At first, the surface nuclei are hyperpolarized using the standard DNP-SENS approach (see Section 3.1). Then, a so-called pulse cooling method is proposed to relay the hyperpolarization to the bulk nuclei (see **Figure 6*a***). In this approach a long delay (tens to hundreds of seconds) is added between polarization of the surface nuclei and the acquisition of the NMR spectra. During this time, spontaneous homonuclear spin diffusion between nuclei with moderate γ propagates the polarization to the bulk. This is only possible owing to very long nuclear relaxation times in the bulk of inorganic solids. Nevertheless, this approach suffers from relatively low DNP enhancements and requires long recycle delays that increase experimental time.

Another approach is to exploit radicals, present in the material or generated by physical or chemical treatment, as endogenous PAs. For example, defects in silicon particles (17, 19, 111, 112) or nanodiamonds (16, 21, 113) associated with dangling bonds can play the role of endogenous PAs. Ha et al. (19) studied hydride-terminated silicon NPs with MAS DNP NMR. While standard exogenous radicals decomposed due to the highly reactive surface of the particles, the use of dangling bonds as endogenous PAs provided moderate DNP enhancements for direct ^{29}Si polarization (19). Notably, thanks to long electron and nuclear relaxation times in nanodiamonds, it was possible to perform endogenous DNP NMR experiments even at room temperature (16).

Endogenous radicals can be generated by exposing materials to γ-rays or by applying electrical discharge (ionizing diluted gas around the sample). As an example, γ-irradiation of fused quartz induced formation of stable radicals. Upon microwave irradiation, these radicals provided tremendous signal enhancement for bulk ^{29}Si nuclei of up to 400 at 110 K (**Figure 6*b***) (15). Noteworthily, sufficient DNP enhancement (up to 150) was achieved even at ambient temperature,

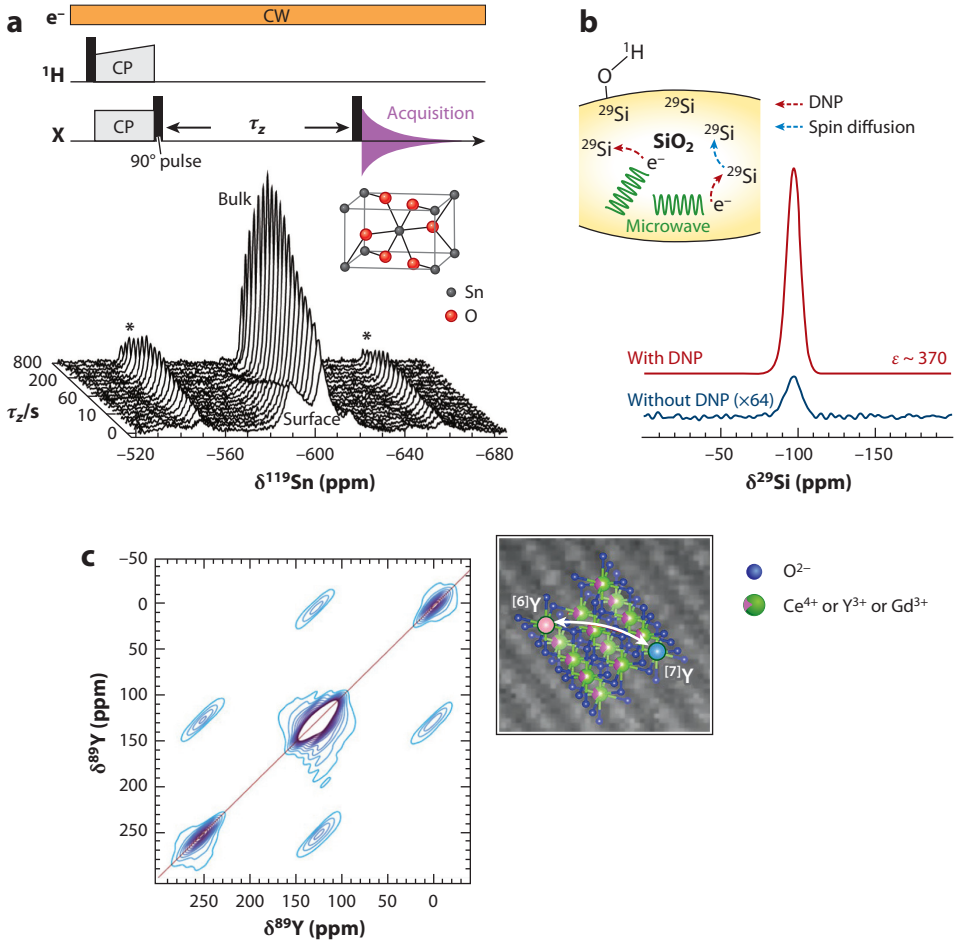

Figure 6

DNP NMR techniques for accessing bulk nuclei of inorganic materials. (*a*, *top*) Pulse cooling sequence for polarization transfer from the surface to the bulk (*black rectangles* represent excitation pulses). (*a*, *bottom*) DNP-enhanced ^{119}Sn CPMAS spectra of SnO_2 acquired as a function of τ_z; spinning sidebands are marked with asterisks. Panel *a* adapted with permission from Reference 108; copyright 2018 American Chemical Society. (*b*) Endogenous DNP exploiting defects in SiO_2, created by γ-irradiation, as PAs. ^{29}Si MAS DNP NMR spectra recorded with (*red*) and without (*dark blue*) microwave irradiation demonstrate enhancement of 370. Panel *b* adapted with permission from Reference 15; copyright 2019 American Chemical Society. (*c*) Analysis of oxygen vacancies distribution in Y-doped CeO_2. Rotational resonance 2D ^{89}Y–^{89}Y MAS NMR spectra recorded with the assistance of DNP from Gd(III) dopants show correlation between Y sites with different coordination numbers. The darker color indicates higher contours. Panel *c* adapted with permission from Reference 119; copyright 2021 American Chemical Society. Abbreviations: CP, cross-polarization; CW, continuous wave; DNP, dynamic nuclear polarization; MAS, magic angle spinning; NMR, nuclear magnetic resonance; PA, polarizing agent.

though very long build-up times were required, making experiments costly in terms of time. The generality of this approach still needs to be verified.

Paramagnetic metal ions containing unpaired electrons can also serve as endogenous PAs. They were explored for DNP applications in the 1950s to 1960s, though the limited instrumentation of

the time hindered their use for materials characterization (7, 114–117). The development of high-field DNP spectrometers and cryogenic MAS probes provoked a new wave of interest in metal-ion PAs. Griffin, Corzilius, and colleagues (9) were the first to demonstrate the efficacy of Gd(III) and Mn(II) complexes as PAs at high field. Mn(II) and Cr(III) were then efficiently used as endogenous PAs in biomolecules and a molecular crystal, respectively (10, 118). Our research group has been developing this approach further, tailoring DNP from paramagnetic metal-ion dopants [metal ions DNP (MIDNP)] for characterizing inorganic materials. These include a broad range of technologically relevant materials for batteries, catalysts, and fuel cells. Currently, a limited number of metal-ion PAs have been reported, namely Mn(II), Fe(III), Gd(III), Cr(III), and V(IV) (10, 12, 13, 69, 119, 120). To be a good PA, a metal ion should possess a sufficiently long electron relaxation time T_{1e}, and its EPR line should be in the range of the magnetic field accessible for the available DNP system. MIDNP enabled hyperpolarization of nuclei in the bulk of the oxides, even those nuclei with extremely low γ, such as ^{89}Y, and/or low NA, such as ^{17}O. This provided valuable structural insights, for example, about the oxygen vacancy distribution in oxide ion conductors (**Figure 6*c***) (119). Another example of MIDNP application for polarizing interfaces in batteries was given in Section 3.1. In most cases where MIDNP was applied, the SE was proposed as the main operating mechanism.

3.4. Polymers

DNP has contributed to organic materials characterization by increasing the efficiency of NMR and expanding its capabilities. In contrast to most inorganic materials, organic compounds contain ^{1}H nuclei; hence, the hyperpolarization created by DNP can spread throughout the bulk by ^{1}H–^{1}H spin diffusion. On the one hand, DNP is not surface-selective in organic materials, but on the other hand, standard exogenous PAs—biradicals operating via CE—provide NMR signal enhancement for the whole sample. In this section, we describe how the development of organic polymers could benefit from NMR with high sensitivity achieved through DNP.

Organic polymers can be tailored to have electrical, magnetic, or optical properties and find applications in energy production and storage, photocatalysis, and separation. Polymers are often amorphous; hence, their structures cannot be determined by X-ray crystallography. Therefore, MAS NMR has always been central to polymer chemistry, as it is applicable to materials without long-range order. Nevertheless, there are cases where MAS NMR fails, such as when the analyzed species are intrinsically diluted. This is the case for the terminal groups of the polymer chain or for diluted monomers. While conventional solid-state NMR can barely detect these, they were clearly identified in DNP-enhanced spectra (121–123); thus, DNP has been proposed to tackle these challenges. MAS DNP NMR coupled with molecular modelling provided unique insights into the polymer backbone conformation and stacking arrangement, the structural features that determine the properties of the polymer (124). Due to the high sensitivity boost, NMR spectra could be recorded even for thin polymeric films with <1 μm thickness (**Figure 7*a***) (124). Moreover, the MAS DNP NMR approach enabled high-throughput characterization of libraries of polymers, where rapid acquisition of solid-state NMR spectra is required (125).

Note that special attention should be given to preparation of polymer samples for DNP studies. In particular, the IWI approach typically used for DNP-SENS of inorganic materials (see Section 3.1) yielded low sensitivity enhancements for polymers (126). Instead, the so-called film casting method was proposed, where the polymer was impregnated with the PA solution followed by solvent evaporation and analysis of the dry sample. Tanaka et al. (127) demonstrated that PA formulation can be chosen on the basis of the polymer swelling properties: Higher swelling volume of the impregnated polymer correlated with better DNP performance. DNP enhancements

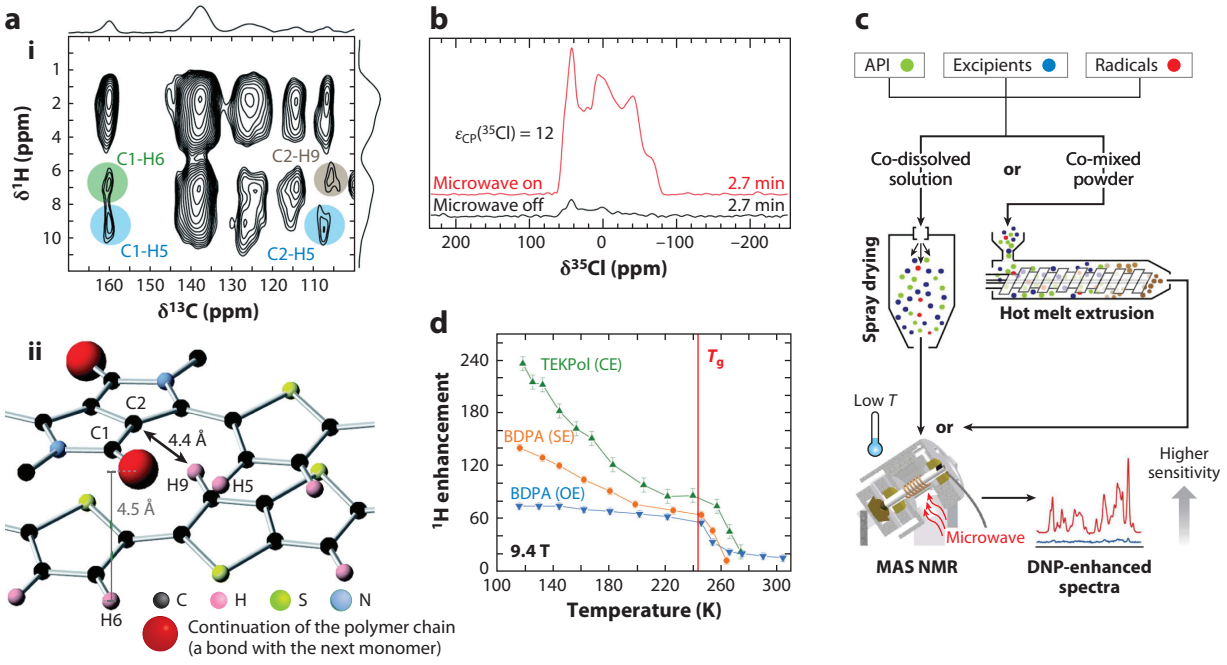

Figure 7

DNP as a tool for studying organic polymers and pharmaceuticals. (*a*, *i*) DNP ^{1}H–^{13}C HETCOR spectrum recorded on drop-cast thin-film polymer showing the close intermolecular proximity and stacking arrangement between two units in the copolymer. (*a*, *ii*) Molecular dynamics–simulated structure of the polymer with calculated distances between the atoms of the two units. Panel *a* adapted with permission from Reference 124; copyright 2017 The Royal Society of Chemistry. (*b*) ^{35}Cl NMR spectra of API isoxsuprine HCl recorded with and without microwave irradiation. Panel *b* adapted with permission from Reference 136; copyright 2016 The Owner Societies. (*c*) Schematic of a dosage preparation containing an API and a PA for in situ NMR analysis of pharmaceuticals. Panel *c* adapted with permission from Reference 131; copyright 2017 American Chemical Society. (*d*) ^{1}H DNP enhancement as a function of sample temperature for radicals operating via CE (*green*), SE (*orange*), and OE (*blue*). Red line indicates the glass transition of *ortho*-terphenyl used as a glass-forming media for APIs. Panel *d* adapted with permission from Reference 138; copyright 2015 American Chemical Society. Abbreviations: API, active pharmaceutical ingredient; CE, cross effect; DNP, dynamic nuclear polarization; HETCOR, heteronuclear correlation; MAS, magic angle spinning; NMR, nuclear magnetic resonance; OE, Overhauser effect; PA, polarizing agent; SE, solid effect.

were significantly improved by oxygen removal from the sample, as this increased proton nuclear relaxation times (128). Note that oxygen removal is generally beneficial in DNP experiments, not only in those on polymers.

3.5. Pharmaceuticals and Composites

As in the case of polymers, where DNP enables detecting minute organic species, a similar scenario is encountered with many pharmaceuticals. Organic compounds play the role of the so-called active pharmaceutical ingredient (API). These APIs often exhibit (pseudo)polymorphism, the ability to have different forms (e.g., hydrate, solvate) and possess different physicochemical properties (stability, solubility, and bioavailability). Undesired polymorphs or impurities present in drugs are potentially dangerous for a patient. Hence, a lot of effort has been invested in developing a tool for structurally characterizing APIs, especially within the solid dosage forms where the API is diluted in a composite. With the emergence of DNP, solid-state NMR spectroscopy has gained greater importance in this field. With the twofold signal enhancement provided by exogenous DNP, it

became possible to record ^{13}C and ^{15}N spectra as well as 2D correlation experiments on API samples at NA (129–133). Besides avoiding a costly and tedious isotopic labeling process, NMR spectra obtained from NA samples are often more informative, owing to the possibilities of long-distance polarization transfers (due to reduced dipolar truncation) (129, 130, 134). As a result, internuclear distances of up to ~7 Å were detected, allowing the observation of noncovalent interactions in solid APIs (134). MAS DNP NMR enabled differentiation of polymorphs of APIs and identification of impurity phases that were present in small quantities in the dosage forms (130, 132, 135). In addition, it provided information about interactions between the API and other components of the pharmaceutical composite—excipients—through high-sensitivity correlation spectra (132, 133). This information is crucial for further optimization of drug formulation. For instance, Zhao et al. (132) utilized DNP-enhanced ^{1}H–^{15}N correlations to measure intermolecular H–N bond lengths, which are an indicator of the interaction between an API and an acidic excipient. Moreover, by analyzing the DNP enhancement as a function of polarization time, it was possible to determine the domain size of the API diluted in the excipient (133).

DNP also enables detecting nuclei in pharmaceuticals other than ^{13}C and ^{15}N. While ^{13}C NMR spectra of dosage forms often display interfering signals from the excipient, ^{35}Cl NMR enhanced by DNP can be used to selectively probe APIs that have been synthesized as HCl salts, even when the Cl content is less than 0.5 wt% (**Figure 7*b***) (136). The DNP formulation was also optimized for ^{19}F nuclei, which are present in 30% of all APIs (137). Noteworthily, in this case polarization transfer occurred via ^{19}F–^{19}F spin diffusion (with no need for ^{1}H).

Finally, careful optimization of the DNP formulation for the pharmaceutical analyte allowed for performing in situ experiments, that is, with the PA being part of a dosage form (**Figure 7*c***) (131), as well as recording MAS DNP NMR spectra at ambient temperature with significant signal enhancements (**Figure 7*d***) (138).

4. CURRENT CHALLENGES AND FUTURE PERSPECTIVES

Despite the significant progress brought by DNP into the field of solid-state NMR spectroscopy and NMR characterization of materials, there are still complex challenges that are yet to be solved. In this section, we discuss the current limitations of DNP and highlight recent examples of studies that address these issues. Finally, we discuss the future directions that can expand DNP methodology, opening additional opportunities for materials characterization.

The first challenge is the application of DNP to chemically reactive materials. The most efficient and commonly used PAs are exogenous organic radicals dissolved in a glass-forming solvent or mixture of solvents (see Section 3). Therefore, to perform the DNP experiment, an analyte has to be exposed to a PA, thus interacting with radical and solvent molecules. This becomes a serious problem when the surface of the material to be analyzed contains reactive species (e.g., active sites on the catalyst surface or reactive species in the SEI layer in electrode materials for batteries). Addition of an organic radical solution may alter the nature of active sites or SEI as well as introduce impurities into the system. Furthermore, the reactive sites can decompose the PAs, leading to insufficient DNP enhancements. Several strategies have been proposed in the literature to overcome the reactivity issue: (*a*) exchanging standard exogenous PAs for endogenous ones, such as intrinsic and generated defects, metal-ion dopants, and lithium dendrites formed inside batteries (see Section 3.3 for more details); (*b*) tailor-made dendritic PAs, in which the bulky dendrimer can reduce the interaction with the analyzed surface (139); (*c*) immobilization of the reactive surface species inside porous materials where they are inaccessible to PA molecules (54, 87); (*d*) the use of acrylamide-based gels as a matrix to stabilize radicals and prevent their reaction with the surface (140); (*e*) incorporation of radicals within the walls of the material (141) or into

the structure of porous covalent organic frameworks (142); and (*f*) adsorption of pyridine on the surface prior to exposing the material to the PA (143). While these approaches have demonstrated the possibility of analyzing reactive species with DNP NMR, they are applicable to specific types of materials and are yet to provide a general route to high DNP enhancements compared with the standard DNP formulations. Therefore, further development and improvement of protected PAs is of great importance for materials research.

Another limitation with commonly used exogenous PAs is accessibility: The organic radicals cannot access target nuclei in certain cases, such as at the buried SEI–metal interface, at the interface between ceramic particles and polymer molecules in solid composite electrolytes, or when the nuclei are part of active sites that are hidden inside small pores and should not be exposed to solvent. Recently, Hope et al. (70) proposed to exploit the conduction electrons of lithium metal as a PA instead of exogenous formulations. Lithium is present in batteries as the anode material, and when deposited in the form of dendrites upon cycling, it can grow and have a very large surface area. Thus, dendrites may have a large interface with the electrolyte resulting in significant SEI formation as well as interfaces within composite electrolytes. The capabilities of this approach are currently under investigation, and the full potential is to be evaluated. Another way to improve accessibility was suggested by Haber et al. (69). A combined exogenous and endogenous DNP study provided unprecedented information about the electrode coating layer: While exogenous PAs probe the outer surface of the coating, endogenous PAs in a form of Fe(III) dopant can access the interface between the coating and the electrode material. Endogenous MIDNP techniques may also be suitable for NMR characterization of microporous zeolite- and MOF-based catalysts, particularly for in situ studies on reagent transformations when the pores should be empty.

Another important research direction is the development of DNP approaches that are suitable for operando/in situ NMR experiments, that is, for monitoring structural changes and ion dynamics in batteries and fuel cells upon electrochemical cycling or for following chemical transformations on a working catalyst. Major efforts were made to design new probes and NMR rotors, making in situ and even operando measurements available for conventional solid-state NMR studies. It is possible nowadays to perform static NMR experiments on a full battery cell cycled inside an NMR magnet over thousands of hours (144, 145). Moreover, clever design of an electrochemical cell within the MAS rotor enabled in situ solid-state NMR analysis of Li species even under MAS conditions (146). Special instrumentation has also been designed for operando MAS NMR studies of chemical reactions: WHiMS rotors (the name is based on the initials of the patent applicants) that are capable of achieving high pressures and high temperatures (147) and constant-flow MAS probes for continuous flowing of gaseous reactants through a catalyst bed and simulation of the realistic catalytic reaction conditions of the flow reactor inside the NMR spectrometer (148–151). If combined with the sensitivity boost provided by DNP, these techniques would be extremely powerful tools for understanding the electrochemical processes inside the working cell or following the chemical transformations on the surface of catalysts.

However, for sufficient sensitivity gains, standard DNP experiments based on the common PA formulations require cryogenic temperatures and hence cannot be performed operando. This low temperature requirement stems from two main considerations: (*a*) the choice of matrix for the radicals, which must stay solid at the experimental temperature, and (*b*) the long electron relaxation times needed for efficient saturation of the electron spin transitions essential for obtaining high signal enhancements. Thus, research efforts should be invested in the development of new PA formulations that are efficient at ambient temperature and higher. Fortunately, there are a few reports showing that DNP at $T > 100$ K is not impossible.

For instance, modification of existing exogenous bis-nitroxide PAs operating via CE by partial deuteration (152) or introduction of bulky ligands (25) led to moderate DNP enhancements at

temperatures up to 200 K, suggesting that continued improvement of radicals should provide large enhancement at higher temperatures. Further work also demonstrated that by choosing a glass-forming medium with a higher glass transition temperature (T_g) than that of the commonly used tetrachloroethane, enhancement of approximately 80 was achieved at the T_g (240 K) (138). Above this temperature, the enhancement rapidly decreased, though it remained approximately 20 up to 273 K, which seems very promising for future operando DNP studies. As mentioned above, the use of Li dendrites enabled the performance of OE-DNP NMR measurements even at ambient temperature, both for static and spinning samples (70). With MIDNP, enhancement of 150 was recently achieved even at higher than ambient temperatures (370 K) (153). This became possible due to the highly symmetric environment of Gd(III) ions doped into CeO_2 (endogenous PAs), resulting in relatively slow electron relaxation, even at 370 K, which is beneficial for the SE DNP.

Noteworthily, the operating DNP mechanism also plays a significant role. In particular, it was found that the DNP efficacy of a carbon-based radical, BDPA, was less sensitive to the temperature via OE than via SE and much less sensitive than the efficacy of CE-DNP with the bis-nitroxide radical TEKPol (**Figure 7*d***) (138). We note, however, that this is not a general observation. Temperature affects all relaxation processes, electron and nuclear, as well as cross-relaxation. Faster electron relaxation at higher temperature would lead to less efficient DNP via all mechanisms, while accelerated cross-relaxation may lead to more efficient OE. Thus, in practice, the interplay between these effects would determine the temperature dependence of the DNP efficacy for a specific PA and mechanism.

An alternative approach for achieving room temperature nuclear hyperpolarization that circumvents the need for long PA relaxation times is the application of coherent polarization transfer schemes. Instead of continuous microwave irradiation, these schemes utilize sequences of microwave pulses that lead to the relatively fast transfer of polarization from the PAs to the nuclei (154–157). Moreover, the development of arbitrary waveform generators, which allow sweeping the microwave frequency over the EPR line of the PA several times during the MAS cycle and maintaining electron polarization, is also promising for high-temperature DNP (158, 159).

Finally, the field of DNP does not stay still, and new mechanisms of hyperpolarization have and will become available for materials characterization. Triplet-DNP draws special attention, as it provides high enhancements even at ambient temperature (see Section 2 for details), though its applications so far have been limited to static measurements and low magnetic fields (30, 160). Further discovery and development of PAs and operating DNP mechanisms are essential to achieve the ultimate goal of performing operando DNP NMR experiments on materials.

5. SUMMARY

Hyperpolarization of nuclei by DNP has opened new horizons in solid-state NMR. Thanks to unprecedented sensitivity enhancement it became possible to acquire NMR spectra within hours that would previously have required years of experimental time. This has broadened the scope of NMR applications in materials characterization: from minute surface species to intermediates of catalytic reactions and from APIs in pharmaceutical composites to unreceptive nuclei in the bulk of inorganic materials. Nevertheless, DNP is still an emerging technique with a lot of untapped potential for materials studies. Further development of new types of PAs, discovery of new mechanisms of polarization transfer, and design of new instrumentation will bring DNP-enhanced NMR to a new level and potentially allow operando/in situ studies of materials under working conditions. With the current ultrafast pace of development in the DNP field, operando studies as well as other comprehensive solid-state NMR experiments are within reach for materials research.

DISCLOSURE STATEMENT

The authors are not aware of any affiliations, memberships, funding, or financial holdings that might be perceived as affecting the objectivity of this review.

ACKNOWLEDGMENTS

I.B.M. acknowledges the Sustainability and Energy Research Initiative (SAERI) fellowship for financial support. M.L. acknowledges support from Israel Science Foundation (grant 1580/17).

LITERATURE CITED

1. Carver TR, Slichter CP. 1953. Polarization of nuclear spins in metals. *Phys. Rev.* 92(1):212–13
2. Bajaj VS, Farrar CT, Hornstein MK, Mastovsky I, Vieregg J, et al. 2003. Dynamic nuclear polarization at 9 T using a novel 250 GHz gyrotron microwave source. *J. Magn. Reson.* 160(2):85–90
3. Chien P-H, Griffith KJ, Liu H, Gan Z, Hu Y-Y. 2020. Recent advances in solid-state nuclear magnetic resonance techniques for materials research. *Annu. Rev. Mater. Res.* 50:493–520
4. Atsarkin VA, Kessenikh AV. 2012. Dynamic nuclear polarization in solids: the birth and development of the many-particle concept. *Appl. Magn. Reson.* 43(1):7–19
5. Thankamony ASL, Wittmann JJ, Kaushik M, Corzilius B. 2017. Dynamic nuclear polarization for sensitivity enhancement in modern solid-state NMR. *Prog. Nucl. Magn. Reson. Spectrosc.* 102–103:120–95
6. Rankin AGM, Trébosc J, Pourpoint F, Amoureux J-P, Lafon O. 2019. Recent developments in MAS DNP-NMR of materials. *Solid State Nucl. Magn. Reson.* 101:116–43
7. Abraham M, McCausland MAH, Robinson FNH. 1959. Dynamic nuclear polarization. *Phys. Rev. Lett.* 2(11):449–51
8. Becerra LR, Gerfen GJ, Bellew BF, Bryant JA, Hall DA, et al. 1995. A spectrometer for dynamic nuclear polarization and electron paramagnetic resonance at high frequencies. *J. Magn. Reson. A* 117(1):28–40
9. Corzilius B, Smith AA, Barnes AB, Luchinat C, Bertini I, Griffin RG. 2011. High-field dynamic nuclear polarization with high-spin transition metal ions. *J. Am. Chem. Soc.* 133(15):5648–51
10. Corzilius B, Michaelis VK, Penzel SA, Ravera E, Smith AA, et al. 2014. Dynamic nuclear polarization of ^{1}H, ^{13}C, and ^{59}Co in a tris(ethylenediamine)cobalt(III) crystalline lattice doped with Cr(III). *J. Am. Chem. Soc.* 136(33):11716–27
11. Chakrabarty T, Goldin N, Feintuch A, Houben L, Leskes M. 2018. Paramagnetic metal-ion dopants as polarization agents for dynamic nuclear polarization NMR spectroscopy in inorganic solids. *ChemPhysChem* 19(17):2139–42
12. Wolf T, Kumar S, Singh H, Chakrabarty T, Aussenac F, et al. 2019. Endogenous dynamic nuclear polarization for natural abundance ^{17}O and lithium NMR in the bulk of inorganic solids. *J. Am. Chem. Soc.* 141(1):451–62
13. Harchol A, Reuveni G, Ri V, Thomas B, Carmieli R, et al. 2020. Endogenous dynamic nuclear polarization for sensitivity enhancement in solid-state NMR of electrode materials. *J. Phys. Chem. C* 124(13):7082–90
14. Corzilius B. 2018. Paramagnetic metal ions for dynamic nuclear polarization. *eMagRes* 7:179–94
15. Carnahan SL, Venkatesh A, Perras FA, Wishart JF, Rossini AJ. 2019. High-field magic angle spinning dynamic nuclear polarization using radicals created by γ-irradiation. *J. Phys. Chem. Lett.* 10(17):4770–76
16. Rej E, Gaebel T, Waddington DEJ, Reilly DJ. 2017. Hyperpolarized nanodiamond surfaces. *J. Am. Chem. Soc.* 139(1):193–99
17. Cassidy MC, Ramanathan C, Cory DG, Ager JW, Marcus CM. 2013. Radical-free dynamic nuclear polarization using electronic defects in silicon. *Phys. Rev. B* 87(16):161306
18. Shimon D, van Schooten KJ, Paul S, Peng Z, Takahashi S, et al. 2019. DNP-NMR of surface hydrogen on silicon microparticles. *Solid State Nucl. Magn. Reson.* 101:68–75
19. Ha M, Thiessen AN, Sergeyev I V, Veinot JGC, Michaelis VK. 2019. Endogenous dynamic nuclear polarization NMR of hydride-terminated silicon nanoparticles. *Solid State Nucl. Magn. Reson.* 100:77–84

20. Riikonen J, Rigolet S, Marichal C, Aussenac F, Lalevée J, et al. 2015. Endogenous stable radicals for characterization of thermally carbonized porous silicon by solid-state dynamic nuclear polarization ^{13}C NMR. *J. Phys. Chem. C* 119(33):19272–78
21. Yoon D, Soundararajan M, Sekatski S, Genoud J, Alberti S, Ansermet JP. 2019. High-field ^{13}C dynamic nuclear polarization in nanodiamond. *J. Phys. Chem. C* 123(34):21237–43
22. Hovav Y, Feintuch A, Vega S. 2012. Theoretical aspects of dynamic nuclear polarization in the solid state – the cross effect. *J. Magn. Reson.* 214:29–41
23. Hu K-N, Yu H, Swager TM, Griffin RG. 2004. Dynamic nuclear polarization with biradicals. *J. Am. Chem. Soc.* 126(35):10844–45
24. Matsuki Y, Maly T, Ouari O, Karoui H, Le Moigne F, et al. 2009. Dynamic nuclear polarization with a rigid biradical. *Angew. Chem. Int. Ed.* 48(27):4996–5000
25. Zagdoun A, Casano G, Ouari O, Schwarzwälder M, Rossini AJ, et al. 2013. Large molecular weight nitroxide biradicals providing efficient dynamic nuclear polarization at temperatures up to 200 K. *J. Am. Chem. Soc.* 135(34):12790–97
26. Can TV, Caporini MA, Mentink-Vigier F, Corzilius B, Walish JJ, et al. 2014. Overhauser effects in insulating solids. *J. Chem. Phys.* 141(6):64202
27. Pylaeva S, Ivanov KL, Baldus M, Sebastiani D, Elgabarty H. 2017. Molecular mechanism of Overhauser dynamic nuclear polarization in insulating solids. *J. Phys. Chem. Lett.* 8(10):2137–42
28. Can TV, Ni QZ, Griffin RG. 2015. Mechanisms of dynamic nuclear polarization in insulating solids. *J. Magn. Reson.* 253:23–35
29. Ji X, Can TV, Mentink-Vigier F, Bornet A, Milani J, et al. 2018. Overhauser effects in non-conducting solids at 1.2 K. *J. Magn. Reson.* 286:138–42
30. Fujiwara S, Hosoyamada M, Tateishi K, Uesaka T, Ideta K, et al. 2018. Dynamic nuclear polarization of metal-organic frameworks using photoexcited triplet electrons. *J. Am. Chem. Soc.* 140(46):15606–10
31. Lesage A, Lelli M, Gajan D, Caporini MA, Vitzthum V, et al. 2010. Surface enhanced NMR spectroscopy by dynamic nuclear polarization. *J. Am. Chem. Soc.* 132(44):15459–61
32. Rossini AJ, Zagdoun A, Lelli M, Lesage A, Copéret C, Emsley L. 2013. Dynamic nuclear polarization surface enhanced NMR spectroscopy. *Acc. Chem. Res.* 46(9):1942–51
33. Zagdoun A, Rossini AJ, Gajan D, Bourdolle A, Ouari O, et al. 2012. Non-aqueous solvents for DNP surface enhanced NMR spectroscopy. *Chem. Commun.* 48(5):654–56
34. Lund A, Casano G, Menzildjian G, Kaushik M, Stevanato G, et al. 2020. TinyPols: a family of water-soluble binitroxides tailored for dynamic nuclear polarization enhanced NMR spectroscopy at 18.8 and 21.1T. *Chem. Sci.* 11(1):2810–18
35. Wisser D, Karthikeyan G, Lund A, Casano G, Karoui H, et al. 2018. BDPA-nitroxide biradicals tailored for efficient dynamic nuclear polarization enhanced solid-state NMR at magnetic fields up to 21.1 T. *J. Am. Chem. Soc.* 140(41):13340–49
36. Wolf P, Valla M, Rossini AJ, Comas-Vives A, Núñez-Zarur F, et al. 2014. NMR signatures of the active sites in Sn-β zeolite. *Angew. Chem. Int. Ed.* 53(38):10179–83
37. Conley MP, Rossini AJ, Comas-Vives A, Valla M, Casano G, et al. 2014. Silica-surface reorganization during organotin grafting evidenced by ^{119}Sn DNP SENS: a tandem reaction of gem-silanols and strained siloxane bridges. *Phys. Chem. Chem. Phys.* 16(33):17822–27
38. Ong T-C, Liao W-C, Mougel V, Gajan D, Lesage A, et al. 2016. Atomistic description of reaction intermediates for supported metathesis catalysts enabled by DNP SENS. *Angew. Chem. Int. Ed.* 55(15):4743–47
39. Venkatesh A, Lund A, Rochlitz L, Jabbour R, Gordon CP, et al. 2020. The structure of molecular and surface platinum sites determined by DNP-SENS and fast MAS ^{195}Pt solid-state NMR spectroscopy. *J. Am. Chem. Soc.* 142(44):18936–45
40. Perras FA, Boteju KC, Slowing II, Sadow AD, Pruski M. 2018. Direct ^{17}O dynamic nuclear polarization of single-site heterogeneous catalysts. *Chem. Commun.* 54(28):3472–75
41. Hamzaoui B, Bendjeriou-Sedjerari A, Pump E, Abou-Hamad E, Sougrat R, et al. 2016. Atomic-level organization of vicinal acid-base pairs through the chemisorption of aniline and derivatives onto mesoporous SBA15. *Chem. Sci.* 7(9):6099–105

42. Klet RC, Kaphan DM, Liu C, Yang C, Kropf AJ, et al. 2018. Evidence for redox mechanisms in organometallic chemisorption and reactivity on sulfated metal oxides. *J. Am. Chem. Soc.* 140(20):6308–16
43. Moroz IB, Larmier K, Liao W-C, Copéret C. 2018. Discerning γ-alumina surface sites with nitrogen-15 dynamic nuclear polarization surface enhanced NMR spectroscopy of adsorbed pyridine. *J. Phys. Chem. C* 122(20):10871–82
44. Perras FA, Wang Z, Kobayashi T, Baiker A, Huang J, Pruski M. 2019. Shedding light on the atomic-scale structure of amorphous silica-alumina and its Brønsted acid sites. *Phys. Chem. Chem. Phys.* 21(35):19529–37
45. Valla M, Rossini AJ, Caillot M, Chizallet C, Raybaud P, et al. 2015. Atomic description of the interface between silica and alumina in aluminosilicates through dynamic nuclear polarization surface-enhanced NMR spectroscopy and first-principles calculations. *J. Am. Chem. Soc.* 137(33):10710–19
46. Rankin AGM, Webb PB, Dawson DM, Viger-Gravel J, Walder BJ, et al. 2017. Determining the surface structure of silicated alumina catalysts via isotopic enrichment and dynamic nuclear polarization surface-enhanced NMR spectroscopy. *J. Phys. Chem. C* 121(41):22977–84
47. Li W, Wang Q, Xu J, Aussenac F, Qi G, et al. 2018. Probing the surface of γ-Al_2O_3 by oxygen-17 dynamic nuclear polarization enhanced solid-state NMR spectroscopy. *Phys. Chem. Chem. Phys.* 20(25):17218–25
48. Hope MA, Halat DM, Magusin PCMM, Paul S, Peng L, Grey CP. 2017. Surface-selective direct ^{17}O DNP NMR of CeO_2 nanoparticles. *Chem. Commun.* 53(13):2142–45
49. Lee D, Duong NT, Lafon O, De Paëpe G. 2014. Primostrato solid-state NMR enhanced by dynamic nuclear polarization: Pentacoordinated Al^{3+} ions are only located at the surface of hydrated γ-alumina. *J. Phys. Chem. C* 118(43):25065–76
50. Johnson RL, Perras FA, Kobayashi T, Schwartz TJ, Dumesic JA, et al. 2016. Identifying low-coverage surface species on supported noble metal nanoparticle catalysts by DNP-NMR. *Chem. Commun.* 52(9):1859–62
51. Klimavicius V, Neumann S, Kunz S, Gutmann T, Buntkowsky G. 2019. Room temperature CO oxidation catalysed by supported Pt nanoparticles revealed by solid-state NMR and DNP spectroscopy. *Catal. Sci. Technol.* 9(14):3743–52
52. Copéret C, Chabanas M, Petroff Saint-Arroman R, Basset J-M. 2003. Homogeneous and heterogeneous catalysis: bridging the gap through surface organometallic chemistry. *Angew. Chem. Int. Ed.* 42(2):156–81
53. Copéret C, Comas-Vives A, Conley MP, Estes DP, Fedorov A, et al. 2016. Surface organometallic and coordination chemistry toward single-site heterogeneous catalysts: strategies, methods, structures, and activities. *Chem. Rev.* 116(2):323–421
54. Pump E, Viger-Gravel J, Abou-Hamad E, Samantaray MK, Hamzaoui B, et al. 2016. Reactive surface organometallic complexes observed using dynamic nuclear polarization surface enhanced NMR spectroscopy. *Chem. Sci.* 8(1):284–90
55. Pump E, Bendjeriou-Sedjerari A, Viger-Gravel J, Gajan D, Scotto B, et al. 2018. Predicting the DNP-SENS efficiency in reactive heterogeneous catalysts from hydrophilicity. *Chem. Sci.* 9(21):4866–72
56. Mohandas JC, Abou-Hamad E, Callens E, Samantaray MK, Gajan D, et al. 2017. From single-site tantalum complexes to nanoparticles of Ta_xN_y and TaO_xN_y supported on silica: elucidation of synthesis chemistry by dynamic nuclear polarization surface enhanced NMR spectroscopy and X-ray absorption spectroscopy. *Chem. Sci.* 8(8):5650–61
57. Eedugurala N, Wang Z, Chaudhary U, Nelson N, Kandel K, et al. 2015. Mesoporous silica-supported amidozirconium-catalyzed carbonyl hydroboration. *ACS Catal.* 5(12):7399–414
58. Gutmann T, Liu J, Rothermel N, Xu Y, Jaumann E, et al. 2015. Natural abundance ^{15}N NMR by dynamic nuclear polarization: fast analysis of binding sites of a novel amine-carboxyl-linked immobilized dirhodium catalyst. *Chem. Eur. J.* 21(9):3798–805
59. Thankamony ASL, Lion C, Pourpoint F, Singh B, Perez Linde AJ, et al. 2015. Insights into the catalytic activity of nitridated fibrous silica (KCC-1) nanocatalysts from ^{15}N and ^{29}Si NMR spectroscopy enhanced by dynamic nuclear polarization. *Angew. Chem. Int. Ed.* 54(7):2190–93
60. Kim SM, Liao W-C, Kierzkowska AM, Margossian T, Hosseini D, et al. 2018. In situ XRD and dynamic nuclear polarization surface enhanced NMR spectroscopy unravel the deactivation mechanism of CaO-based, $Ca_3Al_2O_6$-stabilized CO_2 sorbents. *Chem. Mater.* 30(4):1344–52

61. Akbey Ü, Altin B, Linden A, Özçelik S, Gradzielski M, Oschkinat H. 2013. Dynamic nuclear polarization of spherical nanoparticles. *Phys. Chem. Chem. Phys.* 15(47):20706–16
62. Kobayashi T, Pruski M. 2021. Indirectly detected DNP-enhanced ^{17}O NMR spectroscopy: observation of non-protonated near-surface oxygen at naturally abundant silica and silica-alumina. *ChemPhysChem* 22(14):1441–45
63. Blanc F, Sperrin L, Jefferson DA, Pawsey S, Rosay M, Grey CP. 2013. Dynamic nuclear polarization enhanced natural abundance ^{17}O spectroscopy. *J. Am. Chem. Soc.* 135(8):2975–78
64. Perras FA, Wang Z, Naik P, Slowing II, Pruski M. 2017. Natural abundance ^{17}O DNP NMR provides precise O–H distances and insights into the Brønsted acidity of heterogeneous catalysts. *Angew. Chem. Int. Ed.* 129(31):9293–97
65. Leskes M, Kim G, Liu T, Michan AL, Aussenac F, et al. 2017. Surface-sensitive NMR detection of the solid electrolyte interphase layer on reduced graphene oxide. *J. Phys. Chem. Lett.* 8(5):1078–85
66. Jin Y, Kneusels N-JH, Marbella LE, Castillo-Martínez E, Magusin PCMM, et al. 2018. Understanding fluoroethylene carbonate and vinylene carbonate based electrolytes for Si anodes in lithium ion batteries with NMR spectroscopy. *J. Am. Chem. Soc.* 140(31):9854–67
67. Hestenes JC, Ells AW, Navarro Goldaraz M, Sergeyev IV, Itin B, Marbella LE. 2020. Reversible deposition and stripping of the cathode electrolyte interphase on Li_2RuO_3. *Front. Chem.* 8:681
68. Rosy, Haber S, Evenstein E, Saha A, Brontvein O, et al. 2020. Alkylated $Li_xSi_yO_z$ coating for stabilization of Li-rich layered oxide cathodes. *Energy Storage Mater.* 33:268–75
69. Haber S, Rosy, Saha A, Brontvein O, Carmieli R, et al. 2021. Structure and functionality of an alkylated $Li_xSi_yO_z$ interphase for high-energy cathodes from DNP-ssNMR spectroscopy. *J. Am. Chem. Soc.* 143(12):4694–704
70. Hope MA, Rinkel BLD, Gunnarsdóttir AB, Märker K, Menkin S, et al. 2020. Selective NMR observation of the SEI-metal interface by dynamic nuclear polarisation from lithium metal. *Nat. Commun.* 11(1):2224
71. Lee D, Monin G, Duong NT, Lopez IZ, Bardet M, et al. 2014. Untangling the condensation network of organosiloxanes on nanoparticles using 2D ^{29}Si–^{29}Si solid-state NMR enhanced by dynamic nuclear polarization. *J. Am. Chem. Soc.* 136(39):13781–88
72. Sangodkar RP, Smith BJ, Gajan D, Rossini AJ, Roberts LR, et al. 2015. Influences of dilute organic adsorbates on the hydration of low-surface-area silicates. *J. Am. Chem. Soc.* 137(25):8096–112
73. Kumari B, John D, Hoffmann P, Spende A, Toimil-Molares ME, et al. 2018. Surface enhanced DNP assisted solid-state NMR of functionalized SiO_2 coated polycarbonate membranes. *Z. Phys. Chem.* 232(7–8):1173–86
74. Kumar A, Walder BJ, Kunhi Mohamed A, Hofstetter A, Srinivasan B, et al. 2017. The atomic-level structure of cementitious calcium silicate hydrate. *J. Phys. Chem. C* 121(32):17188–96
75. Lee D, Leroy C, Crevant C, Bonhomme-Coury L, Babonneau F, et al. 2017. Interfacial Ca^{2+} environments in nanocrystalline apatites revealed by dynamic nuclear polarization enhanced ^{43}Ca NMR spectroscopy. *Nat. Commun.* 8:14104
76. Guy ML, van Schooten KJ, Zhu L, Ramanathan C. 2017. Chemisorption of water on the surface of silicon microparticles measured by dynamic nuclear polarization enhanced NMR. *J. Phys. Chem. C* 121(5):2748–54
77. Werner M, Heil A, Rothermel N, Breitzke H, Groszewicz PB, et al. 2015. Synthesis and solid state NMR characterization of novel peptide/silica hybrid materials. *Solid State Nucl. Magn. Reson.* 72:73–78
78. Piveteau L, Ong TC, Rossini AJ, Emsley L, Copéret C, Kovalenko MV. 2015. Structure of colloidal quantum dots from dynamic nuclear polarization surface enhanced NMR spectroscopy. *J. Am. Chem. Soc.* 137(43):13964–71
79. Piveteau L, Ong TC, Walder BJ, Dirin DN, Moscheni D, et al. 2018. Resolving the core and the surface of CdSe quantum dots and nanoplatelets using dynamic nuclear polarization enhanced PASS-PIETA NMR spectroscopy. *ACS Cent. Sci.* 4(9):1113–25
80. Chen Y, Dorn RW, Hanrahan MP, Wei L, Blome-Fernández R, et al. 2021. Revealing the surface structure of CdSe nanocrystals by dynamic nuclear polarization-enhanced ^{77}Se and ^{113}Cd solid-state NMR spectroscopy. *J. Am. Chem. Soc.* 143(23):8747–60

81. Hanrahan MP, Stein JL, Park N, Cossairt BM, Rossini AJ. 2021. Elucidating the location of Cd^{2+} in post-synthetically treated InP quantum dots using dynamic nuclear polarization ^{31}P and ^{113}Cd solid-state NMR spectroscopy. *J. Phys. Chem. C* 125(5):2956–65
82. de Oliveira M, Herr K, Brodrecht M, Haro-Mares NB, Wissel T, et al. 2021. Solvent-free dynamic nuclear polarization enhancements in organically modified mesoporous silica. *Phys. Chem. Chem. Phys.* 23(22):12559–68
83. Grüning WR, Rossini AJ, Zagdoun A, Gajan D, Lesage A, et al. 2013. Molecular-level characterization of the structure and the surface chemistry of periodic mesoporous organosilicates using DNP-surface enhanced NMR spectroscopy. *Phys. Chem. Chem. Phys.* 15(32):13270–74
84. Kobayashi T, Singappuli-Arachchige D, Wang Z, Slowing II, Pruski M. 2017. Spatial distribution of organic functional groups supported on mesoporous silica nanoparticles: a study by conventional and DNP-enhanced ^{29}Si solid-state NMR. *Phys. Chem. Chem. Phys.* 19(3):1781–89
85. Kobayashi T, Slowing II, Pruski M. 2017. Measuring long-range ^{13}C–^{13}C correlations on a surface under natural abundance using dynamic nuclear polarization-enhanced solid-state nuclear magnetic resonance. *J. Phys. Chem. C* 121(44):24687–91
86. Lelli M, Gajan D, Lesage A, Caporini MA, Vitzthum V, et al. 2011. Fast characterization of functionalized silica materials by silicon-29 surface-enhanced NMR spectroscopy using dynamic nuclear polarization. *J. Am. Chem. Soc.* 133(7):2104–7
87. Lafon O, Thankamony ASL, Kobayashi T, Carnevale D, Vitzthum V, et al. 2013. Mesoporous silica nanoparticles loaded with surfactant: low temperature magic angle spinning ^{13}C and ^{29}Si NMR enhanced by dynamic nuclear polarization. *J. Phys. Chem. C* 117(3):1375–82
88. Lund A, Hsieh M-F, Siaw T-A, Han S-I. 2015. Direct dynamic nuclear polarization targeting catalytically active ^{27}Al sites. *Phys. Chem. Chem. Phys.* 17(38):25449–54
89. Zhao EW, Maligal-Ganesh R, Mentink-Vigier F, Zhao TY, Du Y, et al. 2019. Atomic-scale structure of mesoporous silica-encapsulated Pt and PtSn nanoparticles revealed by dynamic nuclear polarization-enhanced ^{29}Si MAS NMR spectroscopy. *J. Phys. Chem. C* 123(12):7299–307
90. Thankamony ASL, Lafon O, Lu X, Aussenac F, Rosay M, et al. 2012. Solvent-free high-field dynamic nuclear polarization of mesoporous silica functionalized with TEMPO. *Appl. Magn. Reson.* 43(1–2):237–50
91. Gajan D, Bornet A, Vuichoud B, Milani J, Melzi R, et al. 2014. Hybrid polarizing solids for pure hyperpolarized liquids through dissolution dynamic nuclear polarization. *PNAS* 111(41):14693–97
92. Gajan D, Schwarzwälder M, Conley MP, Grüning WR, Rossini AJ, et al. 2013. Solid-phase polarization matrixes for dynamic nuclear polarization from homogeneously distributed radicals in mesostructured hybrid silica materials. *J. Am. Chem. Soc.* 135(41):15459–66
93. Vuichoud B, Canet E, Milani J, Bornet A, Baudouin D, et al. 2016. Hyperpolarization of frozen hydrocarbon gases by dynamic nuclear polarization at 1.2 K. *J. Phys. Chem. Lett.* 7(16):3235–39
94. Baudouin D, Van Kalkeren HA, Bornet A, Vuichoud B, Veyre L, et al. 2016. Cubic three-dimensional hybrid silica solids for nuclear hyperpolarization. *Chem. Sci.* 7(11):6846–50
95. Gunther WR, Michaelis VK, Caporini MA, Griffin RG, Román-Leshkov Y. 2014. Dynamic nuclear polarization NMR enables the analysis of Sn-Beta zeolite prepared with natural abundance ^{119}Sn precursors. *J. Am. Chem. Soc.* 136(17):6219–22
96. Wolf P, Valla M, Núñez-Zarur F, Comas-Vives A, Rossini AJ, et al. 2016. Correlating synthetic methods, morphology, atomic-level structure, and catalytic activity of Sn-β catalysts. *ACS Catal.* 6(7):4047–63
97. Harris JW, Liao WC, Di Iorio JR, Henry AM, Ong TC, et al. 2017. Molecular structure and confining environment of Sn sites in single-site chabazite zeolites. *Chem. Mater.* 29(20):8824–37
98. Jain SK, Tabassum T, Li L, Ren L, Fan W, et al. 2021. P-site structural diversity and evolution in a Zeosil catalyst. *J. Am. Chem. Soc.* 143(4):1968–83
99. Berkson ZJ, Messinger RJ, Na K, Seo Y, Ryoo R, Chmelka BF. 2017. Non-topotactic transformation of silicate nanolayers into mesostructured MFI zeolite frameworks during crystallization. *Angew. Chem. Int. Ed.* 56(19):5164–69
100. Xiao D, Xu S, Brownbill NJ, Paul S, Chen L-H, et al. 2018. Fast detection and structural identification of carbocations on zeolites by dynamic nuclear polarization enhanced solid-state NMR. *Chem. Sci.* 9(43):8184–93

101. Fu D, Lucini Paioni A, Lian C, van der Heijden O, Baldus M, Weckhuysen BM. 2020. Elucidating zeolite channel geometry-reaction intermediate relationships for the methanol-to-hydrocarbon process. *Angew. Chem. Int. Ed.* 59(45):20024–30
102. Pourpoint F, Thankamony ASL, Volkringer C, Loiseau T, Trébosc J, et al. 2014. Probing ^{27}Al–^{13}C proximities in metal-organic frameworks using dynamic nuclear polarization enhanced NMR spectroscopy. *Chem. Commun.* 50(8):933–35
103. Rossini AJ, Zagdoun A, Lelli M, Canivet J, Aguado S, et al. 2012. Dynamic nuclear polarization enhanced solid-state NMR spectroscopy of functionalized metal-organic frameworks. *Angew. Chem. Int. Ed.* 51(1):123–27
104. Guo Z, Kobayashi T, Wang L-L, Goh TW, Xiao C, et al. 2014. Selective host-guest interaction between metal ions and metal-organic frameworks using dynamic nuclear polarization enhanced solid-state NMR spectroscopy. *Chem. Eur. J.* 20(49):16308–13
105. Todorova TK, Rozanska X, Gervais C, Legrand A, Ho LN, et al. 2016. Molecular level characterization of the structure and interactions in peptide-functionalized metal-organic frameworks. *Chem. Eur. J.* 22(46):16531–38
106. Kobayashi T, Perras FA, Goh TW, Metz TL, Huang W, Pruski M. 2016. DNP-enhanced ultrawideline solid-state NMR spectroscopy: studies of platinum in metal-organic frameworks. *J. Phys. Chem. Lett.* 7(13):2322–27
107. Carnevale D, Mouchaham G, Wang S, Baudin M, Serre C, et al. 2021. Natural abundance oxygen-17 solid-state NMR of metal organic frameworks enhanced by dynamic nuclear polarization. *Phys. Chem. Chem. Phys.* 23(3):2245–51
108. Björgvinsdóttir S, Walder BJ, Pinon AC, Emsley L. 2018. Bulk nuclear hyperpolarization of inorganic solids by relay from the surface. *J. Am. Chem. Soc.* 140(25):7946–51
109. Björgvinsdóttir S, Moutzouri P, Berruyer P, Hope MA, Emsley L. 2020. Sensitivity enhancements in lithium titanates by incipient wetness impregnation DNP NMR. *J. Phys. Chem. C* 124(30):16524–28
110. Björgvinsdóttir S, Moutzouri P, Walder BJ, Matthey N, Emsley L. 2021. Hyperpolarization transfer pathways in inorganic materials. *J. Magn. Reson.* 323:106888
111. Dementyev AE, Cory DG, Ramanathan C. 2008. Dynamic nuclear polarization in silicon microparticles. *Phys. Rev. Lett.* 100(12):127601
112. Kwiatkowski G, Polyhach Y, Jähnig F, Shiroka T, Starsich FHL, et al. 2018. Exploiting endogenous surface defects for dynamic nuclear polarization of silicon micro- and nanoparticles. *J. Phys. Chem. C* 122(44):25668–80
113. Bretschneider CO, Akbey Ü, Aussenac F, Olsen GL, Feintuch A, et al. 2016. On the potential of dynamic nuclear polarization enhanced diamonds in solid-state and dissolution ^{13}C NMR spectroscopy. *ChemPhysChem* 17(17):2691–701
114. Spence RD, Cowen JA. 1960. Concentration dependence of the polarization and relaxation time of ^{27}Al nuclei in ruby. *J. Chem. Phys.* 32(2):624–25
115. Brun E, Derighetti B, Hundt EE, Niebuhr HH. 1970. NMR of ^{17}O in ruby with dynamic polarization techniques. *Phys. Lett. A* 31(8):416–17
116. Jacquinot JF, Wenckebach WT, Goldman M, Abragam A. 1974. Polarization and NMR observation of ^{43}Ca nuclei in CaF_2. *Phys. Rev. Lett.* 32(20):1096–97
117. Derighetti B, Hafner S, Marxer H, Rager H. 1978. NMR of ^{29}Si and ^{25}Mg In Mg_2SiO_4 with dynamic polarization technique. *Phys. Lett. A* 66(2):150–52
118. Wenk P, Kaushik M, Richter D, Vogel M, Suess B, Corzilius B. 2015. Dynamic nuclear polarization of nucleic acid with endogenously bound manganese. *J. Biomol. NMR* 63(1):97–109
119. Jardón-Álvarez D, Kahn N, Houben L, Leskes M. 2021. Oxygen vacancy distribution in yttrium-doped ceria from ^{89}Y–^{89}Y correlations via dynamic nuclear polarization solid-state NMR. *J. Phys. Chem. Lett.* 12(11):2964–69
120. Jain SK, Yu CJ, Wilson CB, Tabassum T, Freedman DE, Han S. 2021. Dynamic nuclear polarization with vanadium(IV) metal centers. *Chemistry* 7(2):421–35
121. Ouari O, Phan T, Ziarelli F, Casano G, Aussenac F, et al. 2013. Improved structural elucidation of synthetic polymers by dynamic nuclear polarization solid-state NMR spectroscopy. *ACS Macro Lett.* 2(8):715–19

122. Brownbill NJ, Sprick RS, Bonillo B, Pawsey S, Aussenac F, et al. 2018. Structural elucidation of amorphous photocatalytic polymers from dynamic nuclear polarization enhanced solid state NMR. *Macromolecules* 51(8):3088–96
123. Grätz S, de Olivera M, Gutmann T, Borchardt L. 2020. A comprehensive approach for the characterization of porous polymers using ^{13}C and ^{15}N dynamic nuclear polarization NMR spectroscopy. *Phys. Chem. Chem. Phys.* 22(40):23307–14
124. Chaudhari SR, Griffin JM, Broch K, Lesage A, Lemaur V, et al. 2017. Donor-acceptor stacking arrangements in bulk and thin-film high-mobility conjugated polymers characterized using molecular modelling and MAS and surface-enhanced solid-state NMR spectroscopy. *Chem. Sci.* 8(4):3126–36
125. Blanc F, Chong SY, McDonald TO, Adams DJ, Pawsey S, et al. 2013. Dynamic nuclear polarization NMR spectroscopy allows high-throughput characterization of microporous organic polymers. *J. Am. Chem. Soc.* 135(41):15290–93
126. Le D, Casano G, Phan TNT, Ziarelli F, Ouari O, et al. 2014. Optimizing sample preparation methods for dynamic nuclear polarization solid-state NMR of synthetic polymers. *Macromolecules* 47(12):3909–16
127. Tanaka S, Liao W-C, Ogawa A, Sato K, Copéret C. 2020. DNP NMR spectroscopy of cross-linked organic polymers: rational guidelines towards optimal sample preparation. *Phys. Chem. Chem. Phys.* 22(6):3184–90
128. Le D, Ziarelli F, Phan TNT, Mollica G, Thureau P, et al. 2015. Up to 100% improvement in dynamic nuclear polarization solid-state NMR sensitivity enhancement of polymers by removing oxygen. *Macromol. Rapid Commun.* 36(15):1416–21
129. Märker K, Pingret M, Mouesca JM, Gasparutto D, Hediger S, De Paëpe G. 2015. A new tool for NMR crystallography: complete $^{13}C/^{15}N$ assignment of organic molecules at natural isotopic abundance using DNP-enhanced solid-state NMR. *J. Am. Chem. Soc.* 137(43):13796–99
130. Mollica G, Dekhil M, Ziarelli F, Thureau P, Viel S. 2015. Quantitative structural constraints for organic powders at natural isotopic abundance using dynamic nuclear polarization solid-state NMR spectroscopy. *Angew. Chem. Int. Ed.* 54(20):6028–31
131. Ni QZ, Yang F, Can TV, Sergeyev IV, D'Addio SM, et al. 2017. In situ characterization of pharmaceutical formulations by dynamic nuclear polarization enhanced MAS NMR. *J. Phys. Chem. B* 121(34):8132–41
132. Zhao L, Hanrahan MP, Chakravarty P, DiPasquale AG, Sirois LE, et al. 2018. Characterization of pharmaceutical cocrystals and salts by dynamic nuclear polarization-enhanced solid-state NMR spectroscopy. *Cryst. Growth Des.* 18(4):2588–601
133. Rossini AJ, Widdifield CM, Zagdoun A, Lelli M, Schwarzwälder M, et al. 2014. Dynamic nuclear polarization enhanced NMR spectroscopy for pharmaceutical formulations. *J. Am. Chem. Soc.* 136(6):2324–34
134. Märker K, Paul S, Fernández-de-Alba C, Lee D, Mouesca J-M, et al. 2017. Welcoming natural isotopic abundance in solid-state NMR: probing π-stacking and supramolecular structure of organic nanoassemblies using DNP. *Chem. Sci.* 8(2):974–87
135. Veinberg SL, Johnston KE, Jaroszewicz MJ, Kispal BM, Mireault CR, et al. 2016. Natural abundance ^{14}N and ^{15}N solid-state NMR of pharmaceuticals and their polymorphs. *Phys. Chem. Chem. Phys.* 18(26):17713–30
136. Hirsh DA, Rossini AJ, Emsley L, Schurko RW. 2016. ^{35}Cl dynamic nuclear polarization solid-state NMR of active pharmaceutical ingredients. *Phys. Chem. Chem. Phys.* 18(37):25893–904
137. Viger-Gravel J, Avalos CE, Kubicki DJ, Gajan D, Lelli M, et al. 2019. ^{19}F magic angle spinning dynamic nuclear polarization enhanced NMR spectroscopy. *Angew. Chem. Int. Ed.* 58(22):7249–53
138. Lelli M, Chaudhari SR, Gajan D, Casano G, Rossini AJ, et al. 2015. Solid-state dynamic nuclear polarization at 9.4 and 18.8 T from 100 K to room temperature. *J. Am. Chem. Soc.* 137(46):14558–61
139. Liao W-C, Ong T-C, Gajan D, Bernada F, Sauvée C, et al. 2016. Dendritic polarizing agents for DNP SENS. *Chem. Sci.* 8(1):416–22
140. Viger-Gravel J, Berruyer P, Gajan D, Basset J-M, Lesage A, et al. 2017. Frozen acrylamide gels as dynamic nuclear polarization matrices. *Angew. Chem. Int. Ed.* 56(30):8726–30
141. Silverio DL, van Kalkeren HA, Ong T-C, Baudin M, Yulikov M, et al. 2017. Tailored polarizing hybrid solids with nitroxide radicals localized in mesostructured silica walls. *Helv. Chim. Acta* 100(6):e1700101

142. Cao W, Wang WD, Xu H-S, Sergeyev IV, Struppe J, et al. 2018. Exploring applications of covalent organic frameworks: homogeneous reticulation of radicals for dynamic nuclear polarization. *J. Am. Chem. Soc.* 140(22):6969–77
143. Yakimov AV, Mance D, Searles K, Copéret C. 2020. A formulation protocol with pyridine to enable dynamic nuclear polarization surface-enhanced NMR spectroscopy on reactive surface sites: case study with olefin polymerization and metathesis catalysts. *J. Phys. Chem. Lett.* 11(9):3401–7
144. Kayser SA, Mester A, Mertens A, Jakes P, Eichel R-A, Granwehr J. 2018. Long-run in operando NMR to investigate the evolution and degradation of battery cells. *Phys. Chem. Chem. Phys.* 20(20):13765–76
145. Märker K, Xu C, Grey CP. 2020. Operando NMR of NMC811/graphite lithium-ion batteries: structure, dynamics, and lithium metal deposition. *J. Am. Chem. Soc.* 142(41):17447–56
146. Freytag AI, Pauric AD, Krachkovskiy SA, Goward GR. 2019. In situ magic-angle spinning ^{7}Li NMR analysis of a full electrochemical lithium-ion battery using a jelly roll cell design. *J. Am. Chem. Soc.* 141(35):13758–61
147. Walter ED, Qi L, Chamas A, Mehta HS, Sears JA, et al. 2018. Operando MAS NMR reaction studies at high temperatures and pressures. *J. Phys. Chem. C* 122(15):8209–15
148. Hunger M. 2008. In situ flow MAS NMR spectroscopy: state of the art and applications in heterogeneous catalysis. *Prog. Nucl. Magn. Reson. Spectrosc.* 53(3):105–27
149. Hu JZ, Sears JA, Mehta HS, Ford JJ, Kwak JH, et al. 2012. A large sample volume magic angle spinning nuclear magnetic resonance probe for in situ investigations with constant flow of reactants. *Phys. Chem. Chem. Phys.* 14(7):2137–43
150. Arzumanov SS, Stepanov AG. 2013. Parahydrogen-induced polarization detected with continuous flow magic angle spinning NMR. *J. Phys. Chem. C* 117(6):2888–92
151. Wenzel M, Zaheer MA, Issayeva D, Poppitz D, Matysik J, et al. 2021. Flow MAS NMR for in situ monitoring of carbon dioxide capture and hydrogenation using nanoporous solids. *J. Phys. Chem. C* 125(19):10219–25
152. Geiger M-A, Orwick-Rydmark M, Märker K, Franks WT, Akhmetzyanov D, et al. 2016. Temperature dependence of cross-effect dynamic nuclear polarization in rotating solids: advantages of elevated temperatures. *Phys. Chem. Chem. Phys.* 18(44):30696–704
153. Hope MA, Björgvinsdóttir S, Halat DM, Menzildjian G, Wang Z, et al. 2021. Endogenous ^{17}O dynamic nuclear polarization of Gd-doped CeO_2 from 100 to 370 K. *J. Phys. Chem. C* 125(34):18799–809
154. Can TV, Walish JJ, Swager TM, Griffin RG. 2015. Time domain DNP with the NOVEL sequence. *J. Chem. Phys.* 143(5):054201
155. Jain SK, Mathies G, Griffin RG. 2017. Off-resonance NOVEL. *J. Chem. Phys.* 147(16):164201
156. Can TV, Weber RT, Walish JJ, Swager TM, Griffin RG. 2017. Frequency-swept integrated solid effect. *Angew. Chem. Int. Ed.* 56(24):6744–48
157. Tan KO, Yang C, Weber RT, Mathies G, Griffin RG. 2019. Time-optimized pulsed dynamic nuclear polarization. *Sci. Adv.* 5(1):eaav6909
158. Equbal A, Tagami K, Han S. 2019. Pulse-shaped dynamic nuclear polarization under magic-angle spinning. *J. Phys. Chem. Lett.* 10(24):7781–88
159. Gao C, Alaniva N, Saliba EP, Sesti EL, Judge PT, et al. 2019. Frequency-chirped dynamic nuclear polarization with magic angle spinning using a frequency-agile gyrotron. *J. Magn. Reson.* 308:106586
160. Kouno H, Kawashima Y, Tateishi K, Uesaka T, Kimizuka N, Yanai N. 2019. Non-pentacene polarizing agents with improved air stability for triplet dynamic nuclear polarization at room temperature. *J. Phys. Chem. Lett.* 10(9):2208–13